國 立 交 通 大 學

機械工程研究所

碩 士 論 文

應變率對尼龍 6 奈米黏土複合材料

機械性質之探討

Investigating Strain Rate Effect on Mechanical Behaviors of

Nylon 6/clay Nanocomposites

研 究 生 ：黃仁傑

指導教授 ：蔡佳霖 博士

中 華 民 國 九 十 三 年 七 月

應變率對尼龍 6 奈米黏土複合材料機械性質之探討

Investigating Strain Rate Effect on Mechanical Behaviors of Nylon 6/clay Nanocomposites

研 究 生：黃仁傑　　Student：Jen-Chieh Huang

指導教授：蔡佳霖　　Advisor：Jia-Lin Tsai

國 立 交 通 大 學

機 械 工 程 研 究 所

碩 士 論 文

A Thesis

Submitted to Department of Mechanical Engineering

College of Engineering National Chiao Tung University

in partial Fulfillment of the Requirements

for the Degree of

Master

in

Mechanical Engineering

July 2004

Hsinchu, Taiwan, Republic of China

中 華 民 國 九 十 三 年 七 月

應變率對尼龍 6 奈米黏土複合材料機械性質之探討

學生：黃仁傑　　指導教授：蔡佳霖

國立交通大學機械工程研究所

摘　要

本論文主要研究應變率對尼龍 6 奈米黏土複合材料機械行為的影響。乾與濕的奈米複材試片將在本研究中一併做探討。為了解應變率的影響，添加 5%有機黏土的尼龍 6 奈米複材，將以不同的應變率做測試。低應變率的實驗，係藉由液壓萬能材料試驗機進行量測。而在高應變率下，實驗則將利用分離式霍普金森桿(SHPB)來測試。為了得到較準確的動態應力和應變曲線，我們引入脈衝修正技術於 SHPB 測試中。此外，由於濕試片具有低材料機械阻抗的特性，我們採用鋁製的 SHPB 取代傳統鋼製的 SHPB 設備進行動態量測。純尼龍 6 試片也在不同應變率下進行相同的測試，其結果將與奈米複材做比較。由實驗結果觀察，乾尼龍 6 奈米複材試片的應力應變曲線呈現線性區隨著應變率增加而增加的情形。但是在濕試片中，應力應變曲線幾乎呈現非線性的趨勢，而且應變硬化的現象也隨著應變率增加而更加明顯。比較純尼龍 6 與尼龍 6 奈米複材，我們發現在乾的情況下，奈米黏土對於尼龍 6 楊氏係數增強了 32%。相對地，在濕的狀況下，楊氏係數則可以增強到 43%。

Investigating Strain Rate Effect on Mechanical Behaviors of Nylon 6/clay Nanocomposites

Student：Jen-Chieh Huang　　Advisor：Jia-Lin Tsai

Institute of Mechanical Engineering

National Chiao-Tung University

ABSTRACT

This research aims to investigate the rate dependent behavior of nylon 6/clay nanocomposites. Both dry and wet nylon 6/clay nanocomposites were examined in the study. To determine the strain rate effect, the nylon 6 nanocomposites with 5 wt% loading of the organoclay were tested at different strain rates. For low strain rates, the experiment was conducted using hydraulic MTS machine. However, higher strain rate tests were performed using a Split Hopkinson Pressure Bar (SHPB). In order to establish the reliable stress and strain curves of the nanocomposites, a pulse shaper technology was employed in the SHPB tests. Moreover, for the wet specimens with the characteristics of low mechanical impedance, an aluminum SHPB instead of steel SHPB was employed in the high strain rate tests. For comparison purpose, the nylon 6 resin without any organoclay included was also tested in the same manner. Experimental observations reveal that for dry nanocomposites, the linear ranges of the stress and strain curves increase as the strain rate raises. On the other hand, for the wet nanocomposites, the stress and strain curves are almost nonlinear and become strain hardening when the strain rate increases. Comparison of nylon6/clay nanocomposites and pure nylon 6 indicated that the supplement of 5 wt% organoclay in the dry nylon 6 can enhance the Young's modulus to 32% within the tested strain rate ranges. Moreover, for the wet nylon reinforced with organoclay, the increment of Young's modulus can be achieved by 43%.

誌謝

兩年的研究生活在忙碌充實的日子裡度過了，首先感謝指導教授　蔡佳霖博士兩年來專業領域上的悉心指導與栽培，使學生得以順利取得碩士學位，在此致上由衷的謝意。同時也感謝清華大學動機系葉孟考教授、交通大學機械系尹慶中副教授，撥空擔任學生口試委員，給予學生論文研究上的指教，並給予寶貴之意見，在此亦致上無限的感激。

在此並感謝交通大學實習工廠顧文彬老師，莊晰欽老師，在實驗器材製作架設上的協助與指導，使得實驗得以順利進行；玳代企業有限公司宋純德先生，在射出成型、試片製備上大力幫忙；中興大學貴重儀器中心趙佩琪小姐，提供 TEM 影像拍攝與儀器操作之協助；交通大學材料所葉孝蔚學長、李中斌學長，提供 TEM 超薄切片之協助，致上無窮謝意。

感謝實驗室同學王漢偉，一同扶持、互相成長，走過兩年研究生涯，此外同學楊秋華、羅世青、徐家保、陳浩然、李介民、張朝雯、紀建宇、李永洲，室友黃勛維、馬鳴汶，清華大學同學紹耀賢、劉明享，亦在這兩年之中共同譜出美好的研究生活，願他們在未來旅程中，一帆風順，大展宏圖。亦感激實驗室學弟郭濬清、陳奎翰、許世民、曾世華、吳明道、徐茂原，陪我走過後半段研究生活，帶給我歡笑與鼓勵。

此外感激二十多年來父母親，黃共柳先生與沈速端女士，給予無限關懷與鼓勵，使得在求學過程中，無後顧之憂，在此說聲：『爸媽，你們辛苦了！謝謝你們！』

最後感謝容萱，陪伴我走過大學與研究所的時光，帶給我歡笑與淚水，信心與勇氣，總是在難過的時刻，默默的支持鼓勵，雖然緣分將我們帶往不同的道路，但心中期盼，妳，一切安好。

感謝一路走來，在我身旁所有的人，謝謝你們。

目　錄

LIST OF TABLES

LIST OF FIGURES

1、Introduction

1.1 Research motivation

With the latest development of nanotechnology, composites reinforced with nanoclay platelets have been of great interest to many researchers. Nylon 6/clay nanocomposite was one of the nanocomposites which were studied for a decade, and the corresponding mechanical properties were investigated by many researchers. However, few literatures concerning the dynamic response of organoclay nanocomposites were reported. As a result, it is desired to characterize the strain rate effect on mechanical behaviors of the clay-reinforced nanocomposites.

1.2 Paper review

Hopkinson [1] proposed a pioneering method to measure the pressure pulse generated by the detonation of high explosives, which propagated along steel bar into a short bar attached. The total momentum produced by the detonation equals to the transmitted momentum which was trapped in short bar, and the percentage of total momentum trapped in short bar increased with the length of the short bar. Momentum means the time integral of average pressure, and thus the pressure-time relation could be derived by changing the various length of short bar.

Kolsky [2] used a three bars system comprising an anvil, a main bar and an extension bar together with condenser microphones in the cylindrical type and the parallel-plate type, respectively to measure the lateral expansion of the main bar and the displacement at the free end of extension bar. According to these signals were obtained by the condenser microphones, the dynamic stresses and strains of the specimen could be determined. The thin specimen was suggested to minimize the effect of axial inertia, and also the small radius of specimen was recommended to satisfy the radial inertia criterion proposed for high strain rate tests. In order to obtain the reliable stress history, Davies and Hunter [3]

introduced a correction term associated with the axial and radial inertia. It was found that to alleviate the correction term, the optimum specimen size $l = \sqrt{3}\nu_s r$ was proposed where l is specimen length, ν_s is Poisson's ratio and r is specimen radius. Furthermore, they concluded that stress equilibrium in the specimen could be reached if the duration of the input pulse is at least π times than the required time period when a pulse traveling through the specimen.

Lindholm [4] investigated the strain rate sensitivity of three annealed metals, lead, aluminum and copper using the split Hopkinson pressure bar. The true stress-true strain curves were established in terms of flow stress and strain rates on a logarithmic scale, and then a logarithmic function was employed to describe the true stress-strain rate relationship. Bertholf and Karnes [5] examined the effects of the interface friction and the length-to-diameter ratio of specimen on the mechanical behavior of aluminum. With a given strain, the induced contact stresses increase when the friction coefficient is larger. Moreover, it was revealed that the effects of friction were more pronounced when the length-to-diameter ratio of the specimen was smaller. Dioh *et al.* [6] examined the strain rate sensitivity of four thermoplastic materials under low (10^{-4}-$10^{-1}s^{-1}$), intermediate (10^{-1}-10^{2} s^{-1}) and high (10^{2}-10^{4} s^{-1}) strain rates. By following Davies and Hunters' criterion, they concluded that it is critical to choose an appropriate specimen dimension for determining the mechanical behaviors of material with accuracy at high strain rates using a SHPB apparatus. Frew *et al.* [7] discussed the effect of pulse shaping technique on the SHPB test for brittle materials. By adopting annealed or hard C11000 copper as the pulse shapes, they modified the conventional split Hopkinson pressure bar apparatus such that, over most of the test duration, the specimens are in dynamic stress equilibrium and also have nearly constant strain rate.

Ninan *et al.* [8] used the split Hopkinson pressure bar for testing off-axial glass/epoxy composites. The effects of interface friction together with extension-shear coupling

behavior of the off-axis composite specimen were investigated using commercial finite element analysis (FEM) software ANSYS. The almost homogeneous deformation in the off-axis specimen can be achieved with less interface friction. In addition, the effects of the rise time in the incident pulse were characterized. It was indicated that the increasing rise time is effective to extract the reliable dynamic stress-strain curve, which can be accomplished by a thin cupper attached on one end of the incident bar impacted by the strike bar. The history of the SHPB and the associated technique were reviewed by Follansbee [9]

With the development of nanotechnology, the nano-materials, such as carbon nanotubes and organoclay, with high stiffness and strength were considered as the novel reinforcement applicable to composites. The Toyota research center in Japan demonstrated the unprecedented improving in the mechanical performance of the nylon 6/clay nanocomposites [10-15]. In addition, the process about how to prepare well-exfoliated polymer/clay nanocomposites was discussed. Cho and Paul [16] demonstrated that the exfoliated nylon 6/organoclay nanocomposites can be prepared via direct melt compounding using a conventional twin screw extruder.

Dennis *et al.* [17] investigated the importance of the clay surface modification and the mechanism regarding how the clay was melted into the thermoplastic. Two commercial clays (Cloisite 30B and Cloisite 15A) with different surface treatments were added into polyamide 6 using four different types of extruder with multiple screw designs. Experimental results indicated that Cloisite 30B could be much easily delaminated and dispersed in polyamide 6 than Cloisite 15A, implying that the proper chemical treatment of clay surface could assist to fabricate the well-exfoliated nanocomposites. They also found that the degree of dispersion could be affected by the time duration and the corresponding intensity of shear force in the mechanical extruder. Fornes *et al.* [18] compared nylon 6/organoclay nanocomposites based on three different molecular weight grades of nylon 6

which were prepared by melt processing using a twin screw extruder. With the higher molecular weight of polyamides, the nanocomposites exhibit better mechanical properties such as, stiffness and yield strength.

Split Hopkinson Pressure Bar is an effective apparatus for measuring the high strain responses of materials such as metals, ceramics. However, for the materials with low mechanical impedance, a modification is required to obtain a reliable stress and strain curve. In past few years, some researchers have devoted efforts on these issues [19-27].

Chen *et al.* [19] used the aluminum SHPB apparatus together with pulse shaping technique to determine the dynamic compressive stress-strain behaviors of a rigid polyurethane foam with different density under the strain rate range of 1000-5000s^{-1}. The homogeneous deformation of specimen and the dynamic stress equilibrium in the specimen were achieved using the pulse shaper. Sawas *et al.* [20] employed a polymeric split Hopkinson bar to perform the high strain rate test for low-density, low-strength materials such as plastics, rubbers and foams. Since the closer impedance matching between the pressure bars and the specimen materials was achieved, a low noise-to-signal ratio data was obtained in their tests. In addition, the validity of the test results and the viscoelastic data reduction procedure were also demonstrated. Chen *et al.* [21, 22] examined the dynamic responses of low mechanical impedance materials by using high-strength aluminum alloy pressure bars with the hollow transmission bar rather than the conventional steel pressure bars. Due to the lower stiffness of the hollow transmission bar, the noise perturbation on transmitted signal was dramatically reduced. Zhao *et al.* [23, 24] adopted the viscoelastic split Hopkinson pressure bar made by PMMA to investigate the mechanical properties of soft materials such as foams. To obtain the accurate measurements using the viscoelastic bars, the three-dimensional Fourier stationary harmonic wave analysis was carried out for the wave shifting. Based on their studies, it was revealed that the effect of geometrical dispersion in the viscoelastic setup was generally non-negligible.

In order to reduce impedance mismatch for the different directions of the spruce wood specimens, the magnesium bars and steel SHPB were chosen by Widehammar [25] for high strain rate tests. Mahfuz *et al.* [26] replaced the conventional steel transmission bar with polycarbonate transmission bar in the SHPB apparatus. As a result, the strain signal of the transmission bar was enhanced when the low-strength materials were tested. The Hopkinson bar formulations were modified to account for the impedance mismatch between the steel incident bar and the polycarbonate transmission bars. The modified SHPB apparatus was also verified by testing the cylindrical aluminum specimen. Casem *et al.* [27] constructed a polymeric split Hopkinson bar with electromagnetic velocity gages placed in the interfaces between the bars and specimen to obtain the velocities of interfaces. Since the measurement becomes the velocity instead of the strain, the correction for viscoelastic polymeric SHPB apparatus can be eliminated in the analysis, and thus the apparatus is simpler for testing low-strength materials.

1.3 Investigation method

There are two main objectives in this research. The first one is to build up the Split Hopkinson Pressure Bar (SHPB) for high strain rate tests. The fundamental Hopkinson formula was deduced based on one-dimension wave propagation theory. Further, the dispersion effect on the slender bars during the wave propagation was examined by comparing the relative intensity of the frequency detected from two different locations using Fast Fourier Transformation. In order to verify the apparatus suitable for high strain rate tests, the aluminum specimens with the characteristic of strain rate insensitivity were tested at high and low strain rates using SHPB and MTS machine, respectively. Comparison of the experimental results reveals that the SHPB constructed by ourselves are applicable to high strain rate tests.

The second one is to investigate the strain rate effect on mechanical behaviors of clay

reinforced nylon6 nanocomposites by using the SHPB. The nylon 6/clay nanocomposites produced by melt compounding was provided from RTP Company USA and the desired dimension of the specimens were prepared by injection molding. The degree of exfoliation and dispersion in the nylon 6/clay nanocomposites were evaluated using the X-ray diffraction and transmission electron microscope. Since the nylon6 is hygroscopic (moisture sensitive), the moisture effect on mechanical behavior of nylon 6/clay nanocomposites was investigated by immersing the specimens for twenty days. Since the wet samples exhibits the characteristics of low mechanical impedance, an aluminum SHPB was employed instead of steel SHPB for high strain rate test. The Young's modulus of the dry and wet samples were determined from the initial slope of the stress and strain curves measured at different strain rates. For comparison purpose, the unfilled nylon 6 was tested in the same manner. The nanoclay effect and strain rate effect on the Young's modulus of the samples were summarized in this research.

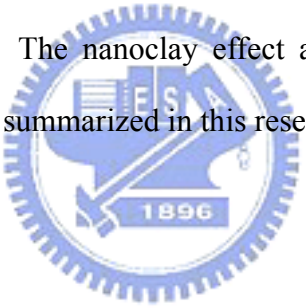

2、 Split Hopkinson pressure bar

2.1 Experimental Setup

The conventional SHPB apparatus consists of a striker bar, an incident bar, a transmission bar and a throw-off bar as showed in Fig. 2.1(a) and (b). There were several considerations for design the split Hopkinson pressure bar to achieve the one-dimensional wave propagation theory as following [9, 28].

1. While the incident bar was impacted by the striker bar, the generated incident wave became complex due to the end effects at the striker bar/incident bar interface. However, these end effects damped quickly while the pulse had propagated about ten bar diameters.
2. The length of incident pressure bar must be long enough to independently obtain the incident and reflected waves.
3. $R/\lambda << 1$. R is the bar radius, and λ is the wavelength of the wave in the bar. In this condition, the axial displacements and stresses were uniform over the cross-section of the bar. In fact, the displacement variation between the surface and center of the bar was less than 5% while the $R/\lambda < 0.1$.

In this study, the steel SHPB apparatus and the aluminum SHPB apparatus were constructed to perform the high strain rate tests. The steel SHPB apparatus was made by tool steel (SKD11). The Young's modulus of tool steel was 206GPa. The lengths of striker bar, incident bar, transmission bar and throw-off bar were 90, 910, 560 and 360 mm, respectively. First, all bars' hardness were increasing around HRC58 by heat treatment to prevent impacting damage. Then the diameter of bars were ground into 13.3 mm to fit the bar supporter made by aluminum. The L/R ratio of the incident bar in this study is about 137 to satisfy the first two considerations, and the L/R ratio of the transmission bar is about 84 to match the second consideration. Moreover, the wavelength of incident wave is about 770 mm in the latter testing, and the R/λ ratio of the pressure bar is much smaller than unity

that satisfies the third consideration. Therefore, it seems that the dimension of the SHPB apparatus in this study satisfies the one-dimensional wave propagation theory. The steel SHPB apparatus was used to investigate the materials which have the stronger mechanical properties. We will study the mechanical properties of aluminum and dry nylon 6 in below section.

However, the aluminum SHPB apparatus was employed to examine the materials, wet nylon 6, with lower mechanical impedances. The aluminum SHPB apparatus which made by aluminum alloy (AL 6061-T6) was also employed to enhance the intensity of the strain gage signals. The Young's modulus of aluminum bars was 67GPa. The lengths of aluminum striker bar, incident bar and transmission bar were 40, 117 and 590 mm, respectively. The diameter of bars of aluminum SHPB apparatus was 13.3 mm which was the same as the diameter of bars of steel SHPB apparatus. The aluminum incident bar was longer than the steel incident bar. It was because that the wavelength of incident wave generated in the aluminum bar was longer than it in the steel incident bar. So the aluminum incident bar needed more length to prevent interfering from the reflected wave.

All pressure bars were aligned by adjusting the aluminum supporter, and this procedure was used to reach one-dimensional wave propagation within the pressure bar and uniaxial compression within the specimen. In addition, the effect of friction is also an important consideration in all kinds of compression testing. In order to reduce the interface friction and mismatch between the specimen and the pressure bar, all bars' cross-sections were machined by the lathe and polished by sandpapers. The petroleum jelly was used to lubricate the specimen/pressure bar interface while testing. A pair of diametrically opposite gages (Micro Measurements EA-13-125AC-350) was mounted on the middle of the incident bar to measure both the incident and reflection wave signals. Similarly, there was also a pair of strain gages mounted on the middle of the transmission bar about at least 20 cm from the specimen/ transmission bar interface to measure the transmitted wave signals.

Gas system consists of a primary steel cylinder, a secondary steel cylinder and a barrel made by hollow stainless tube with inside diameter 13.4 mm. The primary cylinder that contains high-pressure nitrogen gas around 2000psi supplies the secondary steel cylinder the lower pressure gas through a pressure-reducing valve. The secondary steel cylinder was usually empty, but filled with pressure gas while testing begins. The barrel, 170 cm long, was connected with the secondary steel cylinder and supported by aluminum supporters. The barrel provided the striker bar to speed up and restricted the striker bar's direction to impact the incident bar.

Pulse shaping technique was used to generate better rising incident wave, and the more accuracy of dynamic stress-strain curves were obtained [7,8]. The 3 mm copper and 5 mm nylon 6 disks were chosen as pulse shaper for steel SHPB and aluminum SHPB apparatus, respectively.

While the impacting wave propagated along the pressure bars, the strains of the bar were detected by strain gages that mounted on middle of incident bar and transmission bar. The strain signals were transferred to voltage signals by two Wheatstone bridge circuits, and voltage signals were amplified by the Vishay Micro-Measurement Model 2210B signal conditioning amplifier. All voltage signals were obtained by the Tektronix TDS3014B digital oscilloscope.

2.2 Dispersion examination

The dimension of SHPB set-up must be chosen to satisfy the one-dimensional wave propagation theory in this study. For steel SHPB apparatus, the steel incident bar and the steel transmission bar were contacted directly without any specimen at the interface, and the 3 mm copper pulse shaper was attached another free end of the steel incident bar. The incident pulse generated by the striker bar propagated along the incident bar and transmitted into the transmission bar. The wave signals were recorded by the digital

oscilloscope. The incident pulse and the transmitted pulse in time domain were shifted to the instant of time while the incident pulse reached the incident bar/specimen interface. Then these pulse signals were converted to the frequency domain by Fast Fourier Transform (FFT) method. The aluminum SHPB apparatus was also examined by the same procedure with 5 mm nylon 6 pulse shaper.

Fig. 2.2(a) and (b) shows the oscilloscope signals of the incident wave and the transmitted wave on the steel SHPB and aluminum SHPB apparatus, respectively. Then, these signals were shifted to the instant of time while the incident pulse reached the incident bar/transmission bar interface as shown in Fig. 2.3(a) and (b), and these indicated that the pulses in time domain were exactly the same. The FFT results also indicated the perfect matching of frequency spectrums of the incident and transmitted waves in Fig. 2.4(a) and (b). Both results of time domain and frequency domain revealed that the pulse propagated along the SHPB apparatus was satisfying the one-dimensional wave propagation theory in this situation.

2.3 Inertia effect of the specimen

While the incident wave propagated into the specimen, particles of the specimen were accelerated axially and radially. The suggestion that the sufficient thin specimen was used to decrease the axial inertia effects was addressed by Kolsky [2]. He also derived the correction equation (2.1) of recorded signal by introducing the radial kinetic energy.

$$p_m - p_s = \frac{1}{2} \nu_s^2 r^2 \rho_s \frac{d^2 \varepsilon}{dt^2} \tag{2.1}$$

Where p_s is the stress that required to produce a fractional strain ε while no kinetic energy is given to the specimen. The parameter p_m is the measured pressure while the specimen is in the split Hopkinson pressure bar apparatus. The parameter ν_s is Poisson's ratio for the specimen, and r is the specimen radius. The right term due to radial kinetic energy was

vanished while the smaller radius of specimen was employed, and this result indicated that the radial inertia was minimized.

Davies and Hunter [3] introduced a correction term (2.2) associated with the axial and radial inertia to obtain the reliable stress history.

$$\sigma(t)=\sigma_m(t)+\rho_s\left[\frac{L^2}{6}-\nu_s^2\frac{D^2}{8}\right]\frac{d^2\varepsilon(t)}{dt^2} \tag{2.2}$$

In order to alleviate the correction term, the optimum specimen size $L/D=\sqrt{\frac{3}{4}}\nu_s$ is obtained where L is specimen length, ν_s is Poisson's ratio, D is specimen diameter.

In this study, the specimen geometry shown in Fig. 2.5 was chosen for two purposes. One is for approaching the both Kolsky and Davies corrections, another one is for reserving a space to mount the strain gages which recorded the specimen deformation.

Finally, additional important consideration of specimen in the SHPB test is the time t that required for the stress equilibrium within the specimen. The stress equilibrium in the specimen could be reached if the duration of the input pulse is at least π times than the required time period while a pulse traveling through the specimen. The pulse shaper technique introduced in this study provided the longer rising time and the longer duration time of the incident wave, and then the stress equilibrium within the specimen was achieved.

2.4 Fundamental principle

The fundamental principle of the split Hopkinson pressure bar measurement is based on the one-dimensional wave propagation theorem [29]. This implies that a compressive non-dispersive stress wave propagates in a long elastic bar at elastic bar velocity. The impacting of the striker bar at the free end of the incident bar produces a compressive longitudinal incident wave $\varepsilon_i(t)$. Once this compressive longitudinal incident wave

reaches the incident bar/specimen interface, it will separate into two parts, reflected wave and transmitted wave. The reflected wave, $\varepsilon_r(t)$, is a tension wave, and the transmitted wave, $\varepsilon_t(t)$, goes through the specimen and then enters the transmission bar. The incident wave and the reflected wave are recorded by the same strain gages that mounted on the incident bar, and the transmitted wave is also extracted from the strain gages that mounted on the transmission bar.

Usually, we want to approach the time which the incident wave arrives at the incident bar/specimen interface as the reference start of specimen deformation. After the incident wave crosses the incident gages, it needs a time interval Δt_{AB} (A, B are shown in Fig. 2.6) to arrive at the specimen/incident bar interface. The reflected pulse is also recorded by the same set of gages after another time interval Δt_{AB}. Thus, the incident pulse $\varepsilon_i(t)$ and the reflected pulse $\varepsilon_r(t)$ are both recorded by the same set of gages on the incident bar, and then they separate after a time interval $2\Delta t_{AB}$. Thus,

$$\varepsilon_i = \varepsilon_I\left(t - \Delta t_{AB}\right), \tag{2.3}$$

$$\varepsilon_r = \varepsilon_I\left(t + \Delta t_{AB}\right), \tag{2.4}$$

where the strain $\varepsilon_I(t)$ is recorded by the incident gages at any instant of time t.

According to these strain $\varepsilon_i(t)$ and $\varepsilon_r(t)$, the displacement of the incident bar/specimen interface $u_1(t)$ is determined. Similarly, the strain in the transmission bar is also recorded after a time interval Δt_{CD}. This Δt_{CD} is the time that taken by the elastic wave to cross the specimen/transmission bar interface to Gage B as shown in Fig. 2.6. Thus,

$$\varepsilon_t = \varepsilon_T\left(t + \Delta t_{CD}\right), \tag{2.5}$$

where $\varepsilon_T(t)$ is the strain recorded by the transmission gages at any instant of time t.

Then the displacement of specimen/transmission bar interface $u_2(t)$ is derived, and the specimen displacement is calculated as a function of time by analyzing the wave signals. The displacements are represented as follows:

$$u_1(t) = c_o \int_0^t (-\varepsilon_i + \varepsilon_r) d\tau \quad , \tag{2.6}$$

$$u_2(t) = -c_o \int_0^t \varepsilon_t d\tau \quad , \tag{2.7}$$

where C_0 is the longitudinal velocity of the bar.

The average strain is then given by

$$\varepsilon_s = \frac{u_2 - u_1}{l_0} = \frac{c_0}{l_0} \int_0^t (-\varepsilon_t + \varepsilon_i - \varepsilon_r) d\tau \,, \tag{2.8}$$

where l_0 is the original specimen length.

P_1 is compressive force on the incident bar/specimen interface, and P_2 is compressive force on the specimen/the transmission bar interface.

$$P_1 = AE(\varepsilon_i + \varepsilon_r) \,, \tag{2.9}$$

$$P_2 = AE\varepsilon_t \,, \tag{2.10}$$

where A is the cross-section area of the elastic bar in this study.

In the stress equilibrium, $P_1 = P_2$ and $\varepsilon_i(t) + \varepsilon_r(t) = \varepsilon_t(t)$. P_2 is chosen to determine the stress in this study, and the stress in the specimen is given by

$$\sigma_s = \frac{P_2}{A_s} \,, \tag{2.11}$$

where A_s is the cross-section area of the specimen.

The dynamic stress-strain curves are thus extracted from the SHPB experiment data by equation (2.8) and (2.11).

2.5 Verification

Aluminum alloy (AL 6061-T6) was a well-known material with insensitive strain rate. This material characteristic, strain rate insensitivity, was used to verify the reliability of current steel SHPB apparatus. In the present study, MTS 810 system was used to examine

aluminum specimen under quasi-static testing with stroke control 10^{-3}mm/s. In addition, the dynamic tests were also performed using the steel SHPB apparatus. The stress and strain curves which constructed by the quasi-static and dynamic tests were compared to examine the reliability of the SHPB apparatus.

2.5.1 High Strain Rate Test for Aluminum

Aluminum specimens were shaped into 10 mm long and 10 mm in diameter (Fig. 2.5) using the lathe, and a pair of diametrically opposite strain gages (Micro Measurements EA-06-120LZ-120) was mounted on the specimen to obtain the history of its deformation. In order to reduce the effects of friction of the specimen/pressure bar interfaces, all of the specimens' cross-sections were polished by polishing machine with 30μ diamond slurry. Therefore, the aluminum specimens with smooth and paralleled contact loading surfaces were achieved.

The striker bar was pushed by the high gas pressure, 100Psi, to impact the free end of the incident bar which 3 mm thickness copper pulse shaper was attached. The compressive incident wave was generated and propagating along the incident bar. The wave separated into a reflected wave and a transmitted wave while it reached the incident bar/specimen interface. These wave signals were obtained by strain gages mounted on the middle of incident bar and transmission bar. The deformation history of specimen was also recorded by strain gages mounted on it. The strain signals were converted into the voltage signals using Wheatstone bridge circuits, and then the voltage signals were amplified by signal conditioning amplifier. The amplification factors of incident bar channel and transmission bar channel were both set at 600, and the excitation voltages of the Wheatstone bridge circuits were set at 5V. However, the amplification factor of specimen gage signal was set at 50, and the excitation voltage was set at 3V. Finally, all amplified voltage signals were obtained using the digital oscilloscope,

2.5.2 Low Strain Rate Test for Aluminum

In order to avoid the effect of different geometry of specimen, the same dimension of specimen was used to perform the low strain rate test. In addition, the fixture consists of a hemisphere that can slide smoothly in the block with a hemisphere cavity as illustrated in Fig. 2.7(a) and (b). The fixture should be pressed before testing to provide the same parallel plane as the SHPB apparatus, and then it could be used to eliminate potential bending moments under compression testing. Moreover, its contact surfaces were also polished and lubricated by the same procedure that the pressure bar surfaces made. Therefore, the effects of friction were decreased and could be used for quasi-static compression test.

2.5.3 Experimental Results

The recorded original data of SHPB test were shown in Fig. 2.8. The incident and reflected waves on the incident bar, the transmitted wave on the transmission bar, and the specimen strain signal were recorded with sampling rate 10MHz, respectively.

As shown in Fig. 2.9, the origin of all wave signals were shifted to the instant of time that the incident wave arrived the incident bar/specimen interface. The displacements $u_1(t)$ on the incident bar/specimen interface and $u_2(t)$ on the specimen/the transmission bar interface were derived by equations (2.3)~(2.7). Then the specimen strain corresponding to the Hopkinson bar formula was derived. For comparison, the strain signal was also recorded directly by the strain gages mounted on the specimen. The SHPB formula was 15% higher than the experimental result of specimen gage as shown in Fig. 2.10. Hence, the experimental result of specimen gage was chosen to construct the more precise dynamic stress-strain curves. The stresses on the incident bar/specimen and the specimen/transmission bar interfaces were determined by equations (2.9) and (2.10). The stress histories of P_1 and P_2 during the SHPB test were shown in Fig. 2.11. The equilibrium

of P_1 and P_2 indicated that the specimen was homogeneous deformation.

Comparison between the dynamic stress-strain curves from the SHPB test and the static stress-strain curves from the static compression test as shown in Fig. 2.12. The stress strain curves, Young's modulus ,and yielding stress of both static and dynamic testing were almost the same, and these results matched the aluminum characteristic of strain rate insensitivity. It indicated that the procedure used for building up SHPB apparatus and overcoming the difficulties was useful. Consequently, this steel SHPB apparatus could perform the reliable dynamic experiment. Then the dynamic response of nylon 6 and nylon 6/clay nanocomposites will be carried out by this SHPB apparatus in the below section.

3、 Strain rate effect on nylon 6/clay nanocomposites

To investigate the strain rate effect on mechanical behaviors of nylon 6/clay nanocomposites, both nylon 6/clay nanocomposites and neat nylon 6 were tested in compression under high, intermediate and low strain rates. Moreover, both dry and wet specimens were also taken in account to examine the moisture effect on the mechanical responses of the nanocomposites.

3.1 Specimen preparation

The neat nylon 6 (RTP 200A) and nylon 6/clay nanocomposites (RTP 299AX) used in this study were commercially available from RTP Company USA. The organoclay (5.0 wt.%) was blended into nylon 6 via melt compounding process to form nanocomposite pellets. Both neat nylon 6 and nylon 6/clay nanocomposite pellets were dried in vacuum oven at 90 °C for 8hr to eliminate the possible moisture content. The cylindrical specimens with 10 mm in length and 10 mm in diameter were fabricated by means of injection molding. The barrel temperatures in the injection molding machine were set to be 245, 260, and 255 °C from hopper to die, and the mold temperature was equal to 120 °C. The injection pressure and the holding pressure were 11.27MPa and 13.72MPa, respectively.

In order to reduce the contact friction between the specimen and the loading fixture, all specimens were polished using a lapping machine with 25.0μ aluminum oxide powder. In this manner, the specimens with smooth and parallel contact loading surfaces were achieved. The moisture effects of nylon 6 and nylon 6/clay nanocomposites were also discussed in this study. There are two conditions, dry condition and wet condition, of the specimens considered. Before the tests were performed, all dry specimens were kept in a vacuum oven at temperature 50 °C to prevent the moisture absorption. On the other hand,

all wet specimens were kept in water at constant temperature 45℃ to accelerate moisture absorption rate. Fig. 3.1 illustrates the moisture content of the nylon 6 and nylon6/clay nanocomposites recorded daily for 20 days.

3.1.1 X-Ray Diffraction (XRD)

It this section, the Bragg's law was used to determine the d-spacing of the organoclay. The relation of diffraction of X-rays by a crystal was first formulated by W. L. Bragg and is known as Bragg's law.

$$\text{The Bragg's law} \quad : \quad n\lambda = 2d\sin\theta \tag{3.1}$$

where λ is the incident X-ray wavelength, d is the distance of two nearest parallel lattice planes apart, and θ is called the Bragg angle as shown in Fig. 3.2. XRD measurements were conducted on thin neat nylon 6 and nylon 6/clay nanocomposites films (about 0.8 mm thick) using a BEDE D1 diffractometer. The incident X-ray wavelength was 1.54Å, and the scanning speed and the step size were 0.08°/sec and 0.08°, respectively. Fig. 3.3 shows the X-ray diffraction patterns of neat nylon 6 and nylon 6/clay nanocomposites. The XRD peak position at 2θ=0.975° is due to the new crystal phase within nylon 6/clay nanocomposites, and this new crystal phase should be generated from organoclay blended into nylon 6 matrix. By calculating the Bragg's law, the new broad diffraction peak shown in XRD pattern indicated that the organoclay was intercalated into nylon 6 matrix. Then the layer separation of organoclay with d-spacing of 90.5Å was determined.

3.1.2 Transmission Electron Microscope (TEM)

The morphology of nylon 6/clay nanocomposites was imaged using a JEOL 200CX transmission electron microscope at an accelerating voltage of 120 kV. Thin film samples (about 100 nm thick) were cut from injection mold specimens under cryogenic conditions

using a Reichert-Jung Ultracut E microtome.

Fig. 3.4(a) and (b) reveals the extent of exfoliation of nylon 6/clay nanocomposites. The high magnification view in Fig. 3.4(a) shows that the organoclay was blended into nylon 6 matrix in the small area. However, there were several unexfoliated particles of organoclay remained, and there were most intercalated structures in the nanocomposites as shown in Fig. 3.4(b). These results match the XRD results that there was a XRD peak position appear about 0.975°. Both TEM and XRD results reveal that the organoclay was intercalated into nylon 6 matrix.

The morphology of injection molded nanocomposites was investigated in detail using transmission electron microscope (TEM) in the previously articles [18, 30, 31]. It indicates that the dispersed platelets exhibit a high degree of orientation along the injection flow direction. Moreover, the morphology in the skin region of the injection molded nanocomposites exhibits even higher degrees of platelet alignment than in the core region. In this section, the Fig. 3.4(a) shows the high degree of platelet alignment, but the Fig. 3.4(b) doesn't show the same results. It may be due to that the thin-film specimens were cut from the different area of injection specimen.

3.2 Experimental procedure

In this study, the high strain rate test was performed using steel SHPB apparatus for dry specimens and aluminum SHPB apparatus for wet specimens. The intermediate and low strain rate tests were carried out by using MTS 810 system with displacement control.

3.2.1 Dry Specimen Testing

The both dry neat nylon 6 and dry nylon 6/clay nanocomposites were immediately performed under low, intermediate, and high strain rate tests while they left the vacuum oven. The stress and strain relations of dry nylon 6 and dry nylon 6/clay nanocomposites under high strain rate were found using the steel SHPB apparatus. The gas pressure of

100Psi was used to push the steel striker bar, and the compression wave was generated in the steel incident bar with 3mm thickness copper pulse shaper attached on the impact surface. The compression wave signals were obtain by a pair of diametrically opposite gages mounted on the middle of the incident bar and the transmission bar. The amplification factors of incident bar channel and transmission bar channel were both set at 1500. The excitation voltages of the Wheatstone bridge circuits were set at 5V. However, the amplification factor of specimen gage signal was set at 25 under both dry nylon 6 and dry nylon 6/clay specimen test, and the excitation voltages was set at 3V. The sampling rate of oscilloscope was set at 10MHz to record the voltage signals from Wheatstone bridge circuits. The original test data of these materials were recorded by the same way of aluminum specimen test using a digital oscilloscope as shown in Fig. 3.5(a) and (b). Following the same procedure, the incident wave, reflected wave, transmitted wave and specimen gage signals were shifted to same origin of time which the incident pulse reached the incident bar/specimen interface as shown in Fig. 3.6(a) and (b). The histories of P_1 and P_2 during the SHPB tests were shown in Fig. 3.7(a) and (b). The equilibrium of P_1 and P_2 indicated that the nylon 6 and nylon 6/clay nanocomposites specimens were homogeneous deformation. In addition, these results also revealed that P_1 exhibit greater oscillation than P_2. Therefore, P_2 was used to extract the stress in the present high strain rate tests.

The specimen strain corresponding to the Hopkinson formula was obtained from the displacements $u_1(t)$ on the incident bar/specimen interface and $u_2(t)$ on the specimen/the transmission bar interface. However, the strain signal also recorded the histories of specimen deformation by the strain gages mounted on the specimen. Fig. 3.8(a) and (b) show the comparison of the strain histories for dry nylon 6 and dry nylon 6/clay nanocomposites which were obtained by using the Hopkinson bar formula and the strain gage on the specimen, respectively. It is evident that the strain history calculated based on

the Hopkinson bar theory deviates from that directly measured on the specimen. So the gage result was chosen to construct the more accurate stress and strain relations. The stress-strain curves of dry nylon 6 and dry nylon 6/clay nanocomposites were extracted as shown in Fig. 3.9(a) and (b). In this study, the strain rate about 800/s was measured directly from the specimen.

The mechanical behaviors of dry nylon 6 and dry nylon 6/clay nanocomposites under intermediated and low strain rates were performed using MTS 810 system with displacement control at a stroke rate of 1mm/sec and 0.001mm/s, respectively. A self-adjusting device as shown in Fig. 2.7 was used to eliminate potential bending moments and ensure the specimen to be in full contact with the loading surfaces. During these tests, the stress was obtained from the load cell and the corresponding strain was measured from strain gages mounted on the specimens. The stress and strain histories for each test were recorded using LabVIEW, and the sampling rate of low and intermediate test were set at 2Hz and 200Hz, respectively. The strain could be obtained either from the strain gage directly mounted on the specimen (true strain) or the MTS stroke displacements divided by specimen original length (nominal strain). Fig. 3.10(a) and (b) shows the nominal strain curve and the true strain curve for dry nylon 6 and dry nylon6/clay specimen, respectively, tested at the nominal strain rate of 0.1/s. It is evident that the true strain is quite different from the nominal strain and thus the true strain rate is also different from the nominal strain rate. This discrepancy could be ascribed to the application of the self-adjust fixture in the compression test. Therefore, in this study, the true strain curves were employed for the generation of the stress and strain curves and for the evaluation of strain rate as well. For the experiment conducted at nominal strain rate of 0.0001/s, the measured average true strain rate was 8×10^{-5}/s. Furthermore, the average true strain rate was 8×10^{-2}/s corresponding to the experiment at nominal strain rate of 0.1/s.

3.2.2 Wet Specimen Testing

Because the mechanical impedances of wet nylon 6 and wet nylon6/clay nanocomposites are low, the aluminum SHPB apparatus which made by aluminum alloy (6061-T6) was employed in the test to enhance the intensity of the strain signals of the bars. Moreover, pulse shaper technique was utilized to facilitate the homogeneous deformation of the specimens. It results that the reliable stress and strain curves in small strain ranges can be obtained. In this study, the 5 mm thickness of nylon 6 platelet was selected as a pulse shaper for aluminum SHPB tests. The gas pressure of 30Psi was used to initiate the aluminum striker bar, and the same strain gages of steel SHPB apparatus were also mounted on the middle of the aluminum incident bar and transmission bar. The amplification factors of incident bar channel and transmission bar channel were both set at 1000, and the excitation voltage of the Wheatstone bridge circuits were set at 5V. The amplification factor of specimen gage signal was set at 100 and 50 under wet nylon 6 and wet nylon 6/clay specimen test, respectively. The excitation voltages were set at 3V. The sampling rate of oscilloscope was also set at 10MHz. Therefore, the stress-strain curves of wet nylon 6 and wet nylon 6/clay nanocomposites were obtained from tests via aluminum SHPB apparatus.

In order to verify the accuracy of the aluminum SHPB apparatus, the dry nylon 6 and nylon 6/clay nanocomposites were examined using this setup. Fig. 3.11(a) and (b) shows the comparisons of stress and strain curves from the steel SHPB and aluminum SHPB apparatus. It was quite obvious that the testing results from aluminum SHPB apparatus were the same as those from steel SHPB apparatus. Then it indicated that the reliable test results could be obtained by using aluminum SHPB apparatus. Therefore, the aluminum SHPB apparatus could be used to investigate the dynamic mechanical properties of wet nylon 6 specimens. These associated results were presented in Appendix A.

The low and intermediate strain rate tests of wet nylon 6 specimens were performed

by the same procedure of dry specimens. All wet nylon 6 tests were carried out by aluminum SHPB and MTS machine while the moisture absorption of specimens was almost saturate.

3.3 Results and discussion

3.3.1 Dry Specimen Results

The stress and strain curves of dry neat nylon 6 and dry nylon 6/clay nanocomposites at strain rate ranges from 8×10^{-5}/s to 800/s were shown in Fig. 3.12(a) and (b). The constitutive relations exhibit an apparently linear elastic range followed by a nearly perfect plastic behavior. It was shown that, for dry neat nylon 6 and dry nylon 6/clay nanocomposites, the linear elastic ranges increased when the strain rate increases. However, the slopes of the linear portions were almost the same within the tested strain rate range, which indicated that the Young's moduli were not sensitive to strain rate.

Figs. 3.13-3.16 show that the comparison of stress and strain relations of dry neat nylon 6 and dry nylon 6/clay nanocomposites at different strain rate tests, and these results indicated that the Young's modulus and yielding stress of nylon 6/clay were higher than those of neat nylon 6. The Young's modulus for low and intermediate strain tests were determined based on the experimental data with strain range up to 0.5% using a linear function. However, the stress-strain curves of steel SHPB tests under small strain range were more fluctuant than those of aluminum SHPB tests. The Young's modulus of dry nylon 6 and dry nylon 6/clay under high strain rate tests were evaluated from the stress-strain curves of aluminum SHPB tests in this study. The all values of the Young's modulus under different strain rates were summarized in Table 3.1. It reveals that the supplement of 5 wt% organoclay in the dry nylon 6 nanocomposites can improve the stiffness up to 32% with the tested strain ranges.

3.3.2 Wet Specimen Results

Fig. 3.17(a) and (b) shows the stress and strain curves of wet neat nylon 6 and wet nylon 6/clay nanocomposites at strain rate ranges from 8×10^{-5}/s to 500/s. It was shown that these curves are almost nonlinear except that measured at strain rate of 500/s. Theoretically, the Young's modulus should be determined from the slope of the stress and strain curves at the initial portion. However, due to the nonlinearity, it becomes a challenging task to decide the suitable initial strain range for the evaluation of the Young's modulus. In this study, the experimental data with the strain range of 0.05%, 0.1%, 0.2%, and 0.3%, respectively were selected and the corresponding Young's modulus were evaluated by linear curve-fitting as shown, respectively, in Figs 3.18-3.21. It was indicated that for the strain range within 0.05%, the experimental data is lacking and scattering, which prevents the correct interpretation of the Young's modulus. The similar result was observed in the case within strain range of 0.1%. By comparing the results with strain range of 0.2% and 0.3%, it was observed that the Young's modulus is decreasing with the increase of the strain range implying that, in the 0.3% strain level, the nonlinearity is somehow present. In view of the forgoing, the experimental data with strain range of 0.2% was adopted for the determination of the Young's modulus of nanocomposites and nylon 6 specimens with true strain rate up to 0.08/s. More results regarding to the determination of Young's modulus of nylon6 and nylon6/clay nanocomposites in terms of different strain ranges at true strain rate of 8×10^{-5}/s were presented in Appendix B and summarized in Table 3.2. For true strain rate of 0.08/s, based on the experimental data with 0.2% strain level, the Young's modulus of wet nylon6 and wet nylon 6/clay nanocomposites were calculated and illustrated, respectively in Fig. 3.22(a) and (b).

However, for high strain rate, the initial portion (strain less than 0.5%) of the stress and strain curves is quite oscillating and unsuitable for the determination of the Young's modulus. Moreover, experimental observations indicate that the high strain rate

stress-strain curves demonstrate apparently larger linear range than those obtained in the low strain rate. Therefore, we resort the stress and strain curves with strain level up to 0.5% for evaluating the Young's modulus. The associated results for nylon6 and nylon6/clay nanocomposites were shown, respectively in Fig. 3.23(a) and (b). By following the same procedure, the Young's modulus of wet nylon 6 and nylon 6/clay nanocomposites at different strain rates were calculated and the average results were presented in Table 3.3. It was depicted that for the wet nylon6 and wet nylon 6/clay nanocomposites, the Young's modulus increases with the increment of the strain rate. In addition, for each strain rate, the nylon6/clay nanocomposites exhibit higher stiffness than the nylon 6. The enhancement can be achieved up to 43% at the strain rate of 8×10^{-5}/s. Based on out current results, it is interesting to mention that the enhancement seems not to be affected significantly by the strain rate. The complete stress and strain relations of wet nylon 6 and wet nylon 6/clay nanocomposites at three different strain rates were illustrated in Figs. 3.24-3.26. Thus, the inclusion of the organoclay can effectively improve the stiffness of the wet nylon6 in both linear and nonlinear ranges.

3.3.3 Moisture effects

In order to investigate the moisture effect on nylon6/clay nanocomposites, the stress and strain relations shown in Figs. 3.12(b) and 3.17(b) were re-plotted in Figs. 3.27-3.29 in terms of dry and wet samples. It was revealed that for each strain rate, the dry sample always demonstrate superior mechanical response such as stiffness and yielding stress than the wet one. In addition, based on the results summarized in Table 3.1 and Table 3.3, it indicated that, at low strain rate, the Young's modulus of wet nylon6/clay nanocomposites is only 1/4 of that in dry case. Thus, it should be of concern that with the presence of moisture, the mechanical properties of nylon6/clay nanocomposites would be distorted dramatically.

4、Conclusion

In this study, the steel SHPB and aluminum SHPB apparatus were built up and then used for performing high strain rate experiments on the dry and wet samples, respectively. The pulse shaper technology was also introduced to produce a gently rising loading pulse which could facilitate the stress equilibrium and homogeneous deformation of the specimens. As a result, the accurate stress and strain relations, especially in the small strain range, can be extracted from SHPB tests. The following is the summary of the dry and wet nylon6/clay nanocomposites tested at different strain rates.

- For dry nylon6/clay nanocomposites, the Young's modulus is not affected significantly by strain rate at the strain rate up to 800/s. However, the linear elastic limit increases when the strain rate increases.

- For wet nylon6/clay nanocomposites, the constitutive curves are almost nonlinear and the Young's modulus increases along with the increase of strain rate. In addition, moisture content dramatically reduces the stiffness of nylon6/clay nanocomposites.

- The supplement of 5 wt% organoclay in the dry nylon 6 can enhance the Young's modulus to 32 % within the tested strain rate ranges. Moreover, the enhancement can be up to 43% in the wet nylon 6 samples.

5、References

[1] Hopkinson, B. 1914 “A Method of Measuring the Pressure Produced in the Detonation of High Explosives or by the Impact of Bullets,” *Philosophical Transactions of the Royal Society of London*, A213, pp. 437-456

[2] Kolsky, H. 1949 “An Investigation of the Mechanical Properties of Materials at very High Rates of Loading,” *Proceedings of the Physical Society. Section B*, Vol. 62, pp. 676-701.

[3] Davies, E. D. H. and Hunter, S. C. 1963 “The Dynamic Compression Testing of Solids by the Method of the Split Hopkinson Pressure Bar,” *Journal of the mechanics and physics of solids*, Vol.11, pp. 155-178.

[4] Lindholm, U. S. 1964 “Some Experiments with the Split Hopkinson Pressure Bar,” *Journal of the mechanics and physics of solids,* Vol. 12, pp. 317-335.

[5] Bertholf, L. D. and Karnes, C. H. 1975 “Two-Dimensional Analysis of the Split Hopkinson Pressure Bar System,” *Journal of the mechanics and physics of solids*; Vol. 23, pp. 1-19.

[6] Dioh, N. N., Leevers, P. S. and Williams, J. G. 1993 “Thickness Effects in Split Hopkinson Pressure Bar Tests,” *Polymer*; Vol.34, No. 20, pp. 4230-4234.

[7] Frew, D. J, Forrestal, M. J. and Chen W. 2002 “Pulse Shaping Techniques for Testing Brittle Materials with a Split Hopkinson Pressure Bar,” *Experimental Mechanics*, Vol. 42, No. 1, pp. 93-106

[8] Ninan, L., Tsai, J. and Sun, C. T. 2001 “Use of Split Hopkinson Pressure Bar for Testing Off-axis Composites,” *International Journal of Impact Engineering,* Vol. 25, pp. 291-313.

[9] Follansbee, P. S. 1978 “High Strain Rate Compression Testing,” *Metals Handbook*, Ninth Edition, American Society for Metals. Materials Park, Vol. 8, pp.190-207.

[10] Kojima, Y., Usuki, A., Kawasumi, M., Okada, A., Kurauchi, T., Kamigaito, O. 1993 “Synthesis of Nylon 6-Clay Hybrid by Montmorillonite Intercalated with ε-Caprolactam,” *Journal of Polymer Science: Part A: Polymer Chemistry*, Vol. 31, pp. 983-986.

[11] Usuki, A., Kojima, Y., Kawasumi, M., Okada, A., Fukushima, Y., Kurauchi, T., Kamigaito, O. 1993 "Synthesis of Nylon 6-Clay Hybrid," *Journal of Materials Research*, Vol. 8, No. 5, pp. 1179-1184.

[12] Kojima, Y., Usuki, A., Kawasumi, M., Okada, A., Kurauchi, T., Kamigaito, O., Kaji, K. 1994 "Fine Structure of Nylon 6-Clay Hybrid," *Journal of Polymer Science: Part B: Polymer Physics*, Vol. 32, pp. 625-630.

[13] Kojima, Y., Usuki, A., Kawasumi, M., Okada, A., Kurauchi, T., Kamigaito, O., Kaji, K. 1995 "Novel Preferred Orientation in Injection-Molded Nylon 6-Clay Hybrid," *Journal of Polymer Science: Part B: Polymer Physics*, Vol. 33, pp. 1039-1045.

[14] Usuki, A., Koiwai, A., Kojima, Y., Kawasumi, M., Okada, A., Kurauchi, T., Kamigaito, O. 1995 "Interaction of Nylon 6-Clay Surface and Mechanical Properties of Nylon 6-Clay Hybrid," *Journal of Applied Polymer Science*, Vol. 55, pp. 119-123.

[15] Okada, A. and Usuki, A. 1995 "The Chemistry of Polymer-Clay Hybrids," *Materials Science and Engineering: C*, Vol. 3, pp. 109-115.

[16] Cho, J.W. and Paul, D.R. 2001 "Nylon 6 Nanocomposites by Melt Compounding," *Polymer*, Vol. 42, pp. 1083-1094.

[17] Dennis, H.R., Hunter, D.L., Chang, D., Kim, S., White, J.L. Cho, J.W. Paul, D.R. 2001 "Effect of Melt Processing Conditions on the Extent of Exfoliation in Organoclay-Based Nanocomposites," *Polymer*, Vol. 42, pp. 9513-9522.

[18] Fornes, T.D., Yoon, P.J., Keskkula, H., Paul, D.R. 2001 "Nylon 6 Nanocomposites: the Effect of Matrix Molecular Weight," *Polymer*, Vol. 42, pp. 9929-9940.

[19] Chen, W., Lu, F. and Winfree, N. 2002 "High-Strain-Rate Compressive Behavior of a Rigid Polyurethane Foam with Various Densities," *Experimental Mechanics*, Vol. 42, No. 1, pp. 65-73.

[20] Sawas, O., Brar, N. S. and Brockman, R. A. 1998 "Dynamic Characterization of Compliant Materials Using an All-polymeric Split Hopkinson Bar," *Experimental*

Mechaincs, Vol. 38, No. 3, pp. 204-210.

[21] Chen, W., Zhang, B. and Forrestal, M. J. 1999 "A Split Hopkinson Bar Technique for Low-impedance Materials," *Experimental Mechaincs*, Vol. 39, No. 2, pp. 1-5.

[22] Chen, W., Lu, F., Frew, D. J. and Forrestal, M. J. 2002 "Dynamic Compression Testing of Soft Materials," *Journal of Applied Mechanicals*, Vol. 69, pp. 214-223.

[23] Zhao, H., Gary, G. and Klepaczko, J. R. 1997 "On The Use of A Viscoelastic Split Hopkinson Pressure Bar," *International Journal of Impact Engineering,* Vol. 19, No. 4, pp. 319-330.

[24] Zhao, H. 1997 "Testing of Polymeric Foams at High and Medium Strain Rates," *Polymer Testing,* Vol. 16, pp. 507-516.

[25] Widehammar, S. 2004 "Stress-Strain Relationships for Spruce Wood: Influence of Strain Rate, Moisture Content and Loading Direction," *Experimental Mechanics,* Vol. 44, No. 1, pp.44-48.

[26] Mahfuz, H., Mamun, W. A., Haque, A., Turner, S. and Mohamed, H., Jeelani, S. 2000 "An Innovative Technique for Measuring the High Strain Rate Response of Sandwich Composites," *Composite Structures,* Vol. 50, pp.279-285.

[27] Casem, D. T., Fourney, W. L. and Chang, P. 2003 "A Polymeric Split Hopkinson Pressure Bar Instrumented with Velocity Gages," *Experimental Mechanics,* Vol. 43, No. 4, pp.420-427.

[28] Follansbee, P. S. and Frantz, C. 1983 "Wave Propagation in the Split Hopkinson Pressure Bar," *Journal of Engineering Materials and Technology*, Vol. 105, pp.61-66.

[29] Graff, K. F. 1975 *Wave motion in elastic solids*, Ohio State University, pp. 75-134.

[30] Fornes, T. D. and Paul, D. R. 2003 "Modeling properties of nylon6/clay nanocomposites using composite theories," *Polymer*, Vol. 44, pp. 4993-5013.

[31] Yoon, P. J., Fornes, T. D. and Paul, D. R. 2002 "Thermal expension behavior of nylon 6 nanocomposites," *Polymer*, Vol. 43, pp. 6727-6741.

TABLE 3.1. Young's modulus of dry nylon 6 and dry nylon 6/clay nanocomposites under different strain rates

Material	High (800/s)	Intermediate(8×10^{-2}/s)	Low (8×10^{-5}/s)
Nylon 6	3.1GPa	3.1GPa	3.1GPa
Nylon 6/clay	4.1GPa	4.1GPa	4.1GPa
Enhance ratio	32%	32%	32%

TABLE 3.2. Young's modulus of wet nylon 6 and wet nylon 6/clay nanocomposites of different strain ranges under low strain rate tests

Strain range	0.05%	0.1%	0.2%	0.3%
Nylon 6(Test1)	0.42GPa	0.71GPa	0.75GPa	0.73GPa
Nylon 6(Test2)	0.6GPa	0.74GPa	0.72GPa	0.7GPa
Nylon 6/clay(Test1)	1.36GPa	1.16GPa	1.06GPa	1.07GPa
Nylon 6/clay(Test2)	0.73GPa	0.81GPa	1.04GPa	1.17GPa

TABLE 3.3. Young's modulus of wet nylon 6 and wet nylon 6/clay nanocomposites under different strain rates

Material	High (500/s)	Intermediate(8×10^{-2}/s)	Low (8×10^{-5}/s)
Nylon 6 (moisture)	1.2GPa (8.27%)	1.0GPa (8.52%)	0.735GPa (8.49%)
Nylon 6/clay (moisture)	1.6GPa (7.48%)	1.24GPa (7.64%)	1.05GPa (7.65%)
Enhance ratio	33%	24%	43%

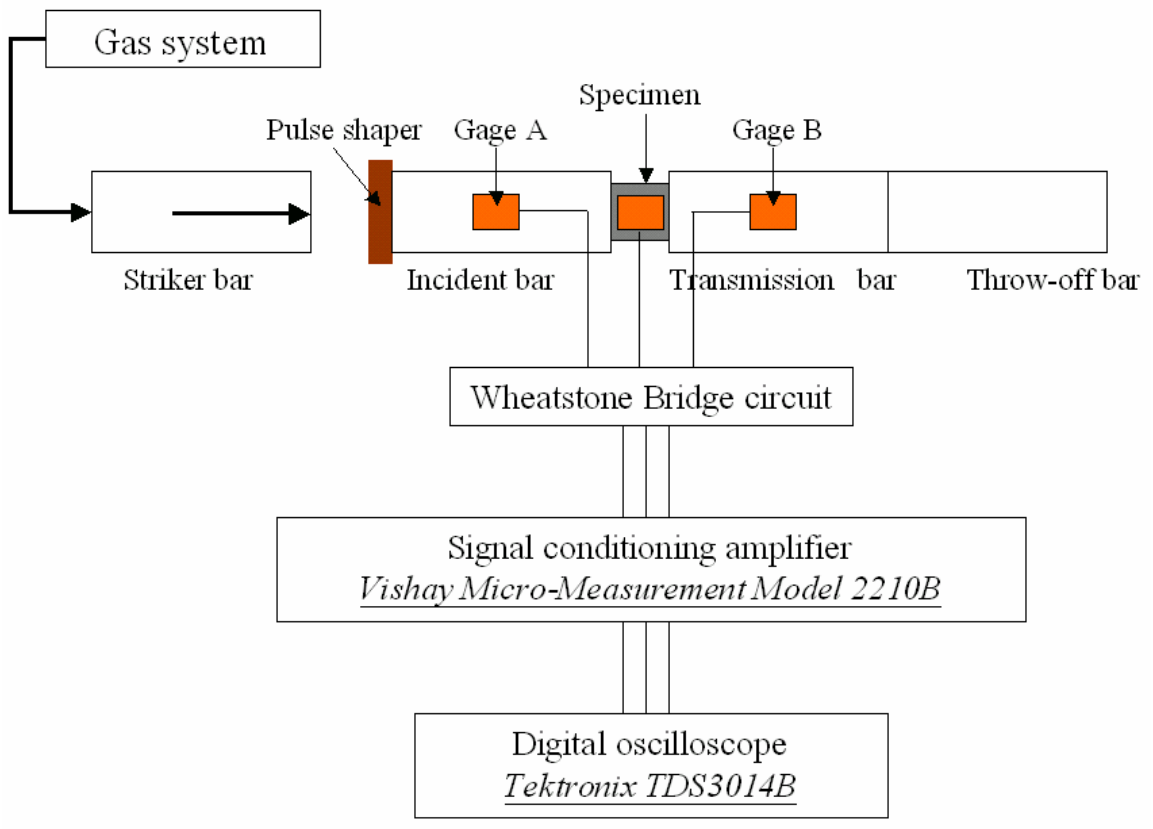

Fig. 2.1(a) Schematic of Split Hopkinson Pressure Bar apparatus.

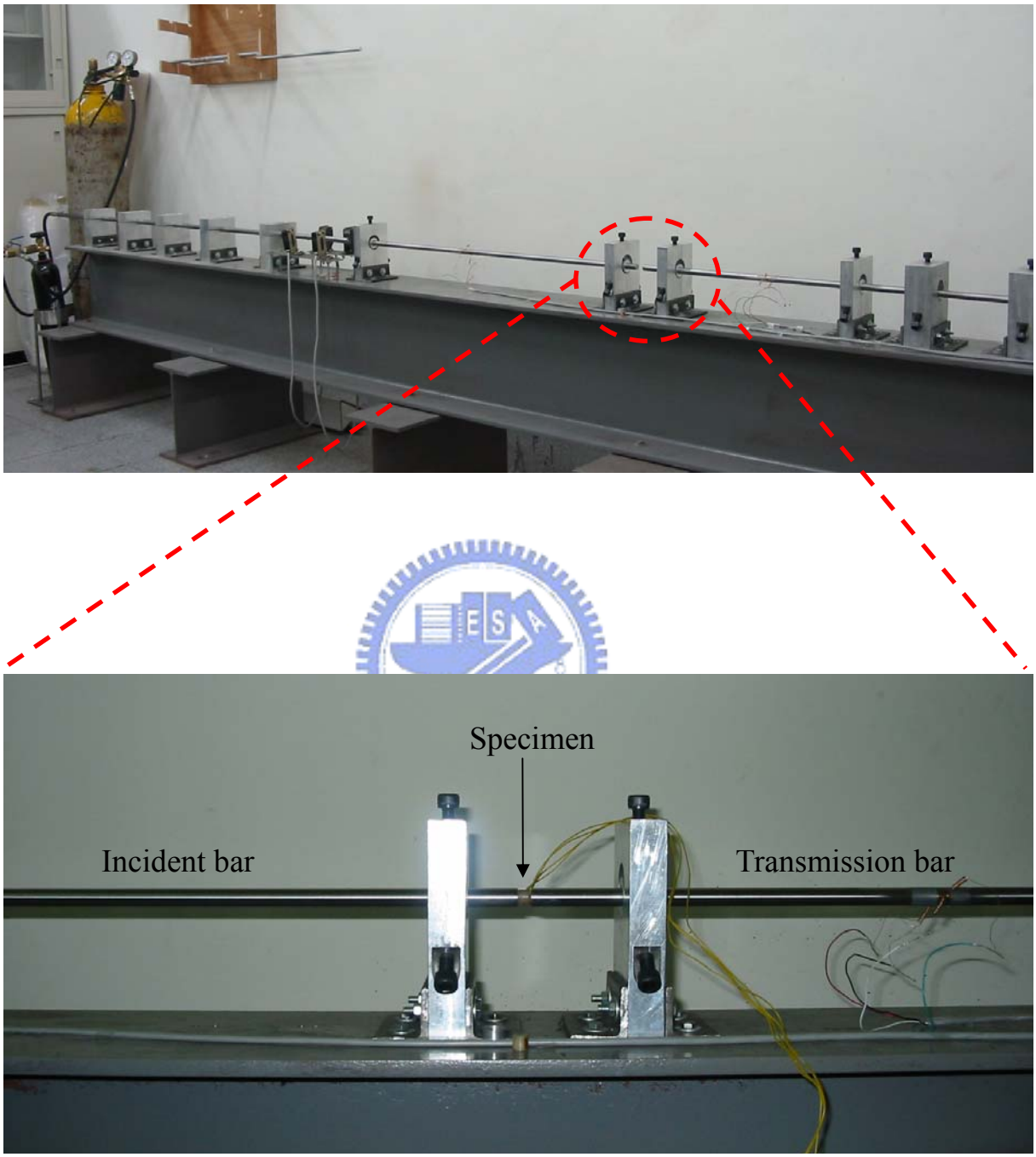

Fig. 2.1(b) Photo of Split Hopkinson Pressure Bar

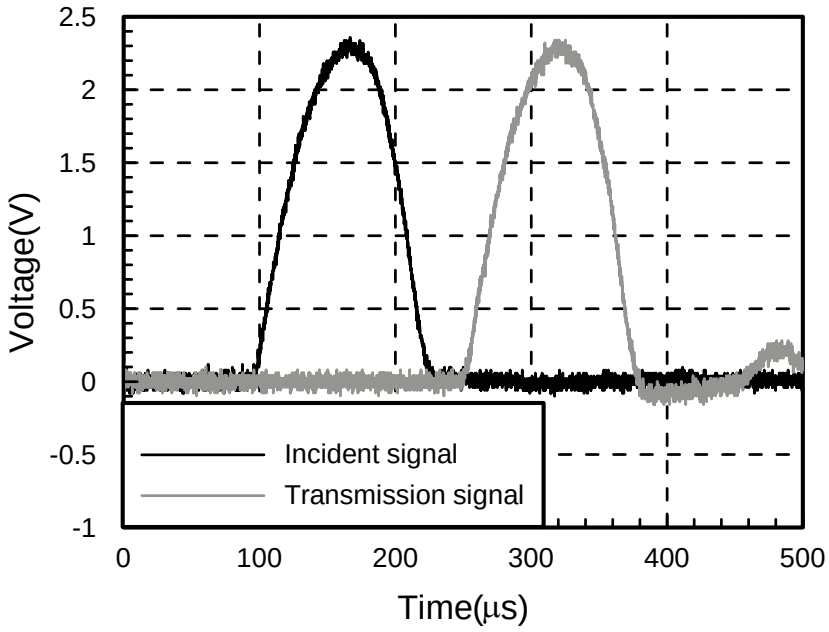

Fig. 2.2(a) Incident wave signal and transmitted wave signal of steel SHPB were shaped by 3 mm copper pulse shaper.

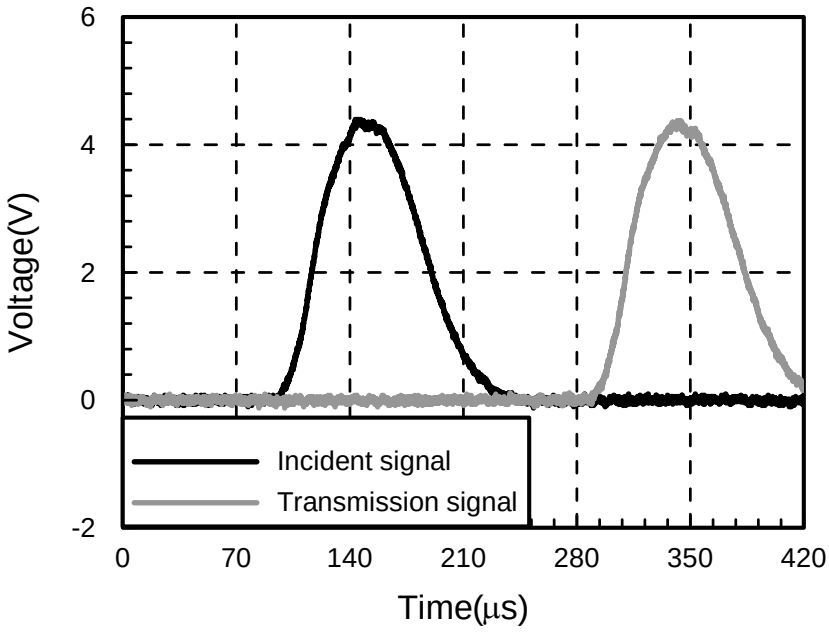

Fig. 2.2(b) Incident wave signal and transmitted wave signal of aluminum SHPB were shaped by 5 mm nylon 6 pulse shaper.

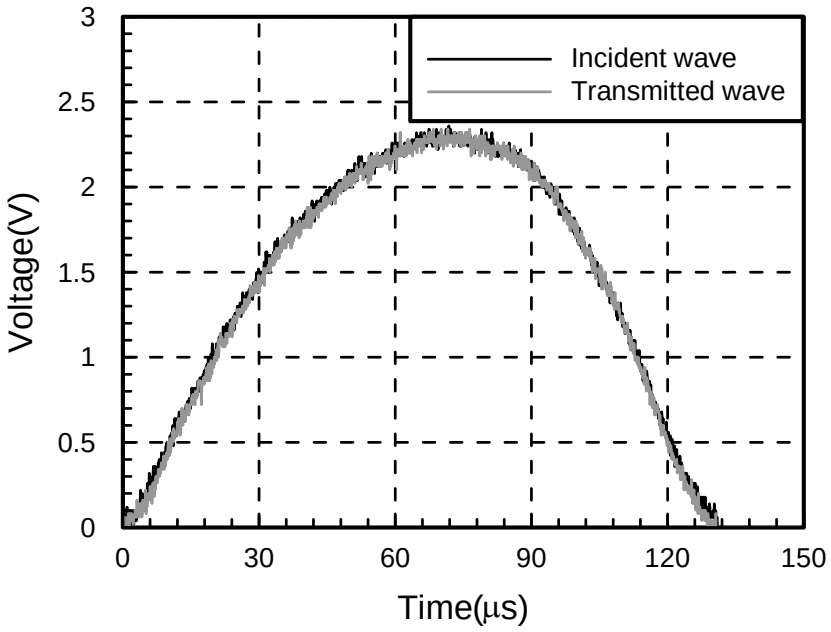

Fig. 2.3(a) The shaped incident and transmitted wave signals were shifted to the instant of time while the incident wave reached the incident bar/specimen interface (Steel SHPB).

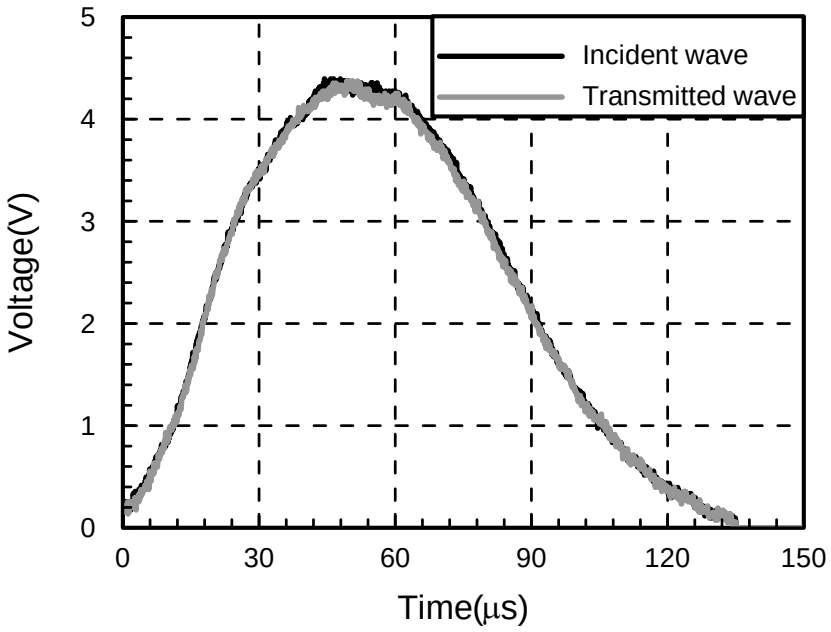

Fig. 2.3(b) The shaped incident and transmitted wave signals were shifted to the instant of time while the incident wave reached the incident bar/specimen interface (Aluminum SHPB).

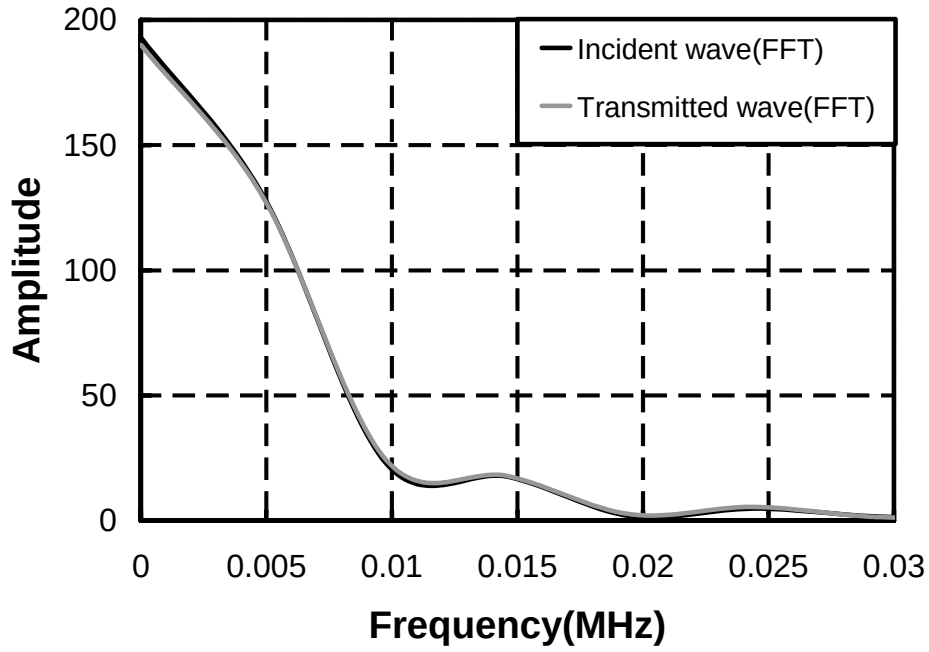

Fig. 2.4(a) The FFT result of the incident wave signal was modified by pulse shaper technique (Steel SHPB).

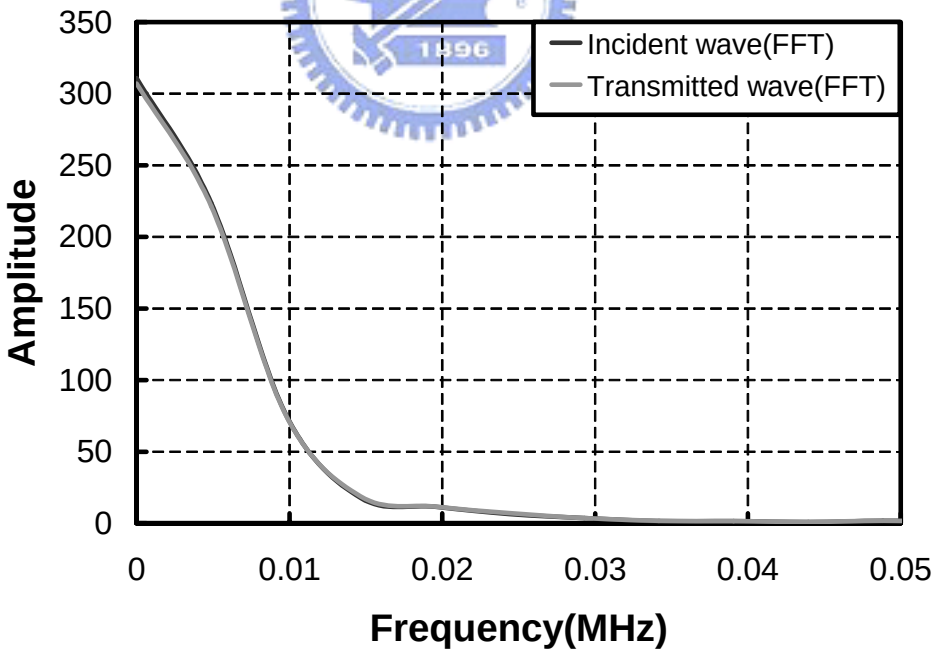

Fig. 2.4(b) The FFT result of the incident wave signal was modified by pulse shaper technique (Aluminum SHPB).

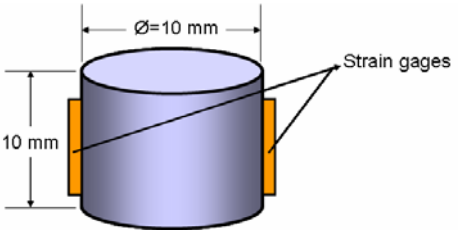

Fig. 2.5. Schematic of the SPBH testing specimens.

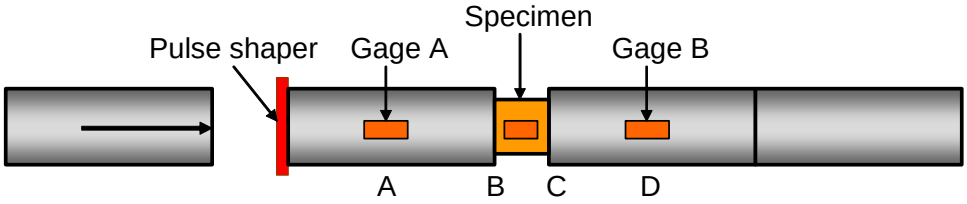

Fig. 2.6. Schematic of Split Hopkinson Pressure Bar

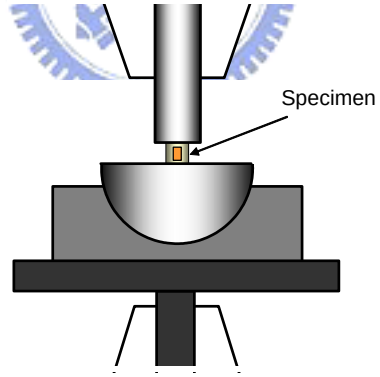

Fig. 2.7(a) Schematic of MTS compression test fixture

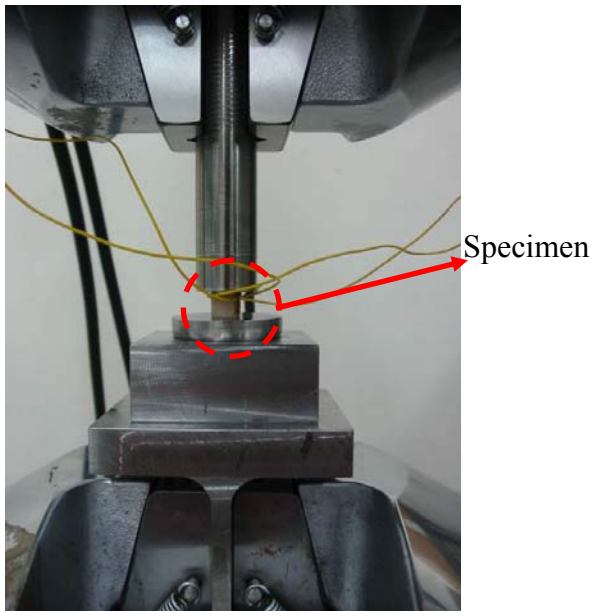

Fig. 2.7(b) Photo of MTS compression test fixture

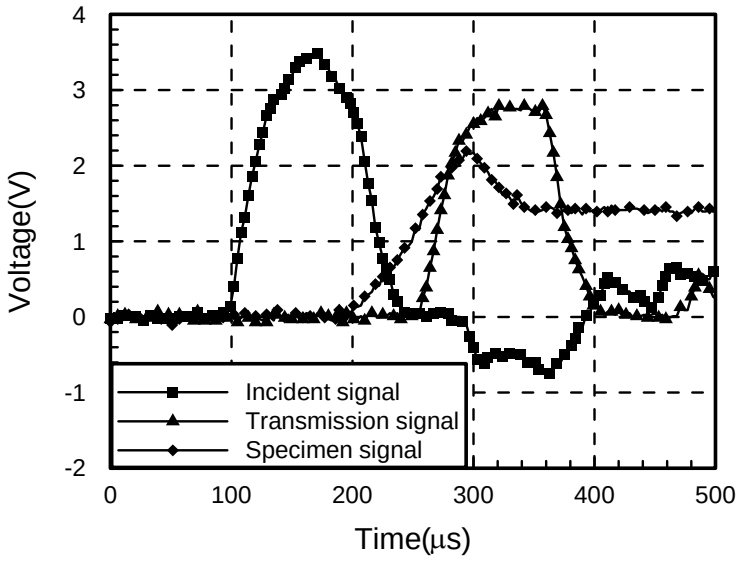

Fig. 2.8. Strain gage signals recorded in SHPB test for aluminum specimen.

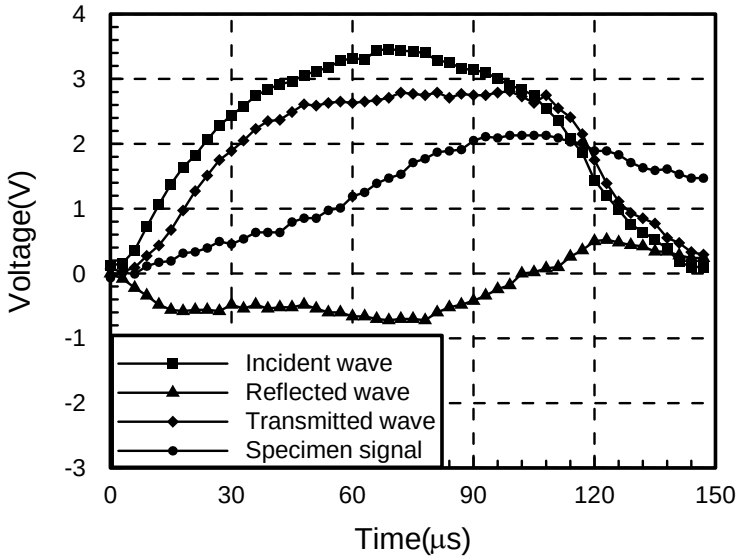

Fig. 2.9. Time shift for strain gage signals recorded in SHPB test for aluminum specimen.

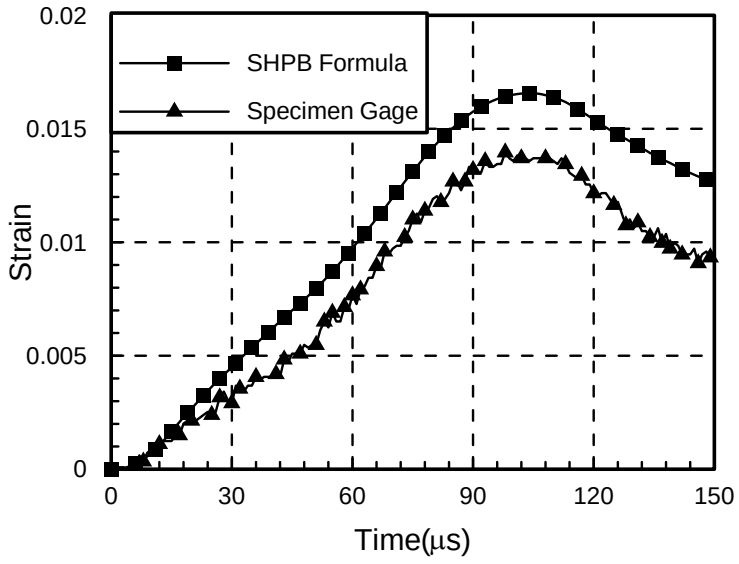

Fig. 2.10. Strain history obtained from Hopkinson bar formula and strain gage signals for aluminum specimen in SHPB tests.

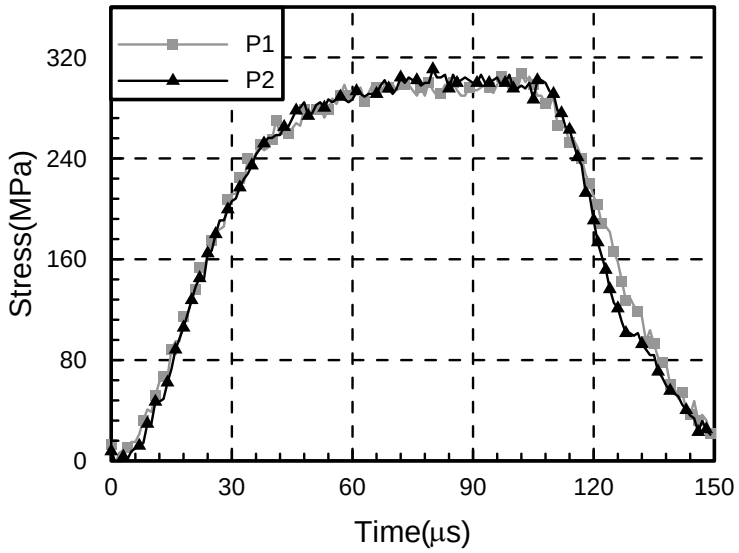

Fig. 2.11. Time histories of the contact stresses for aluminum specimen in SHPB tests.

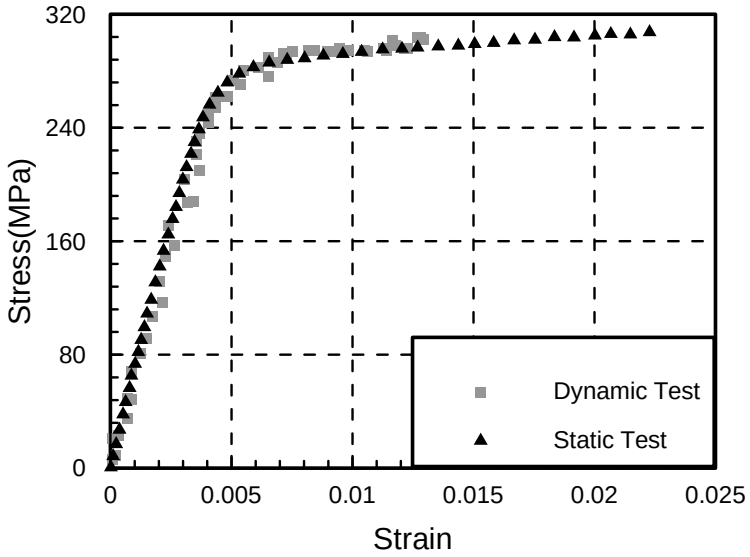

Fig. 2.12. Comparison of dynamic and static stress-strain curves of aluminum specimen.

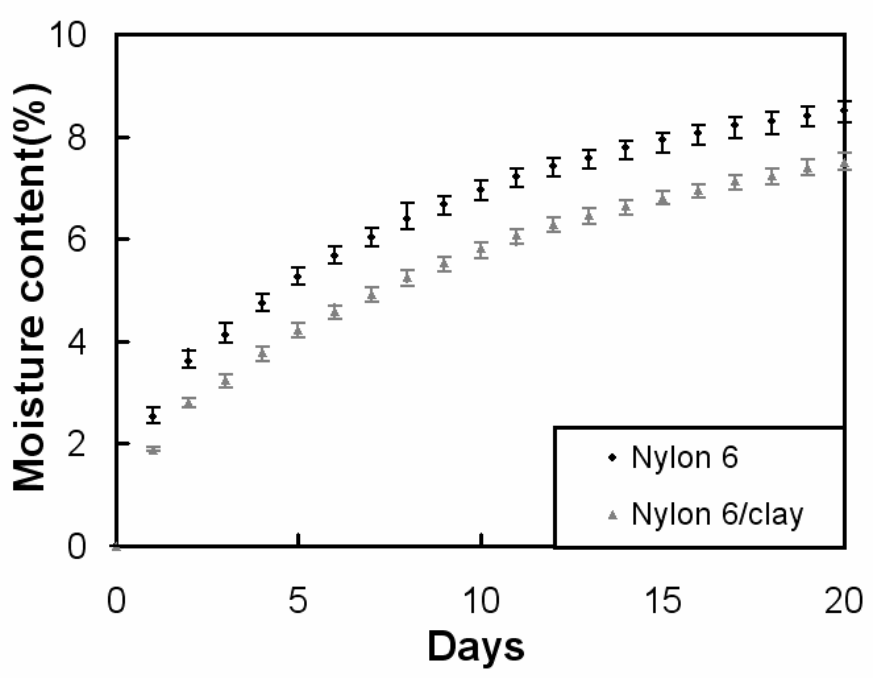

Fig. 3.1. The moisture increment of wet nylon 6 and wet nylon 6/clay nanocomposites.

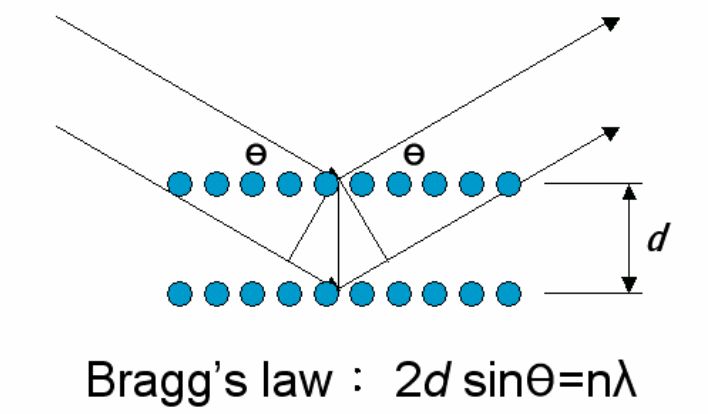

Fig. 3.2. Diffraction of X-rays by a crystal.

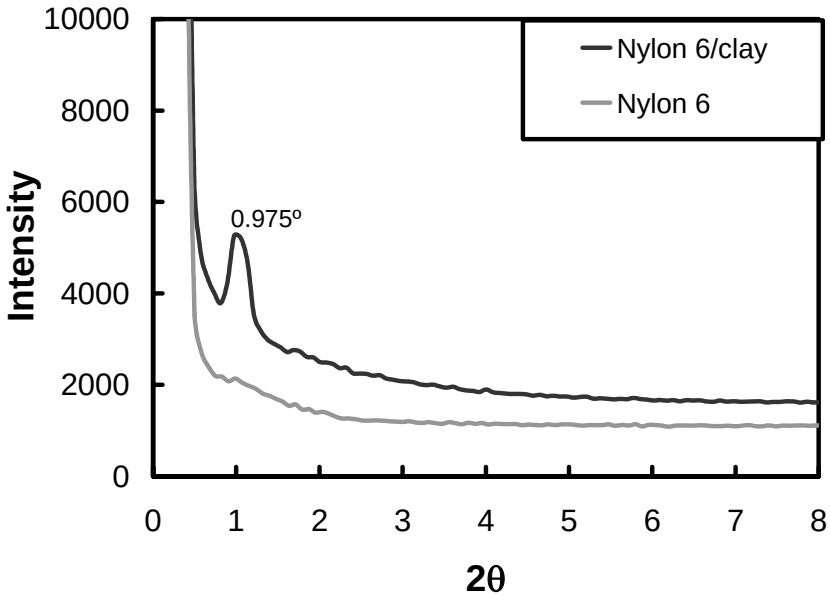

Fig. 3.3. X-ray diffraction scans for neat nylon 6 and nylon 6/clay nanocomposites prepared by melt compounding process.

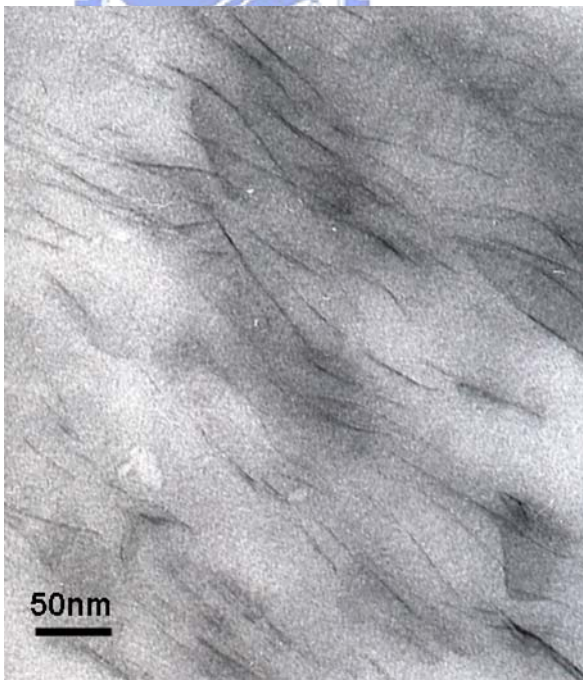

Fig. 3.4(a) TEM photomicrographs of nylon 6/clay nanocomposites prepared by melt compounding process and shaped by injection molding machine in 100,000 magnification.

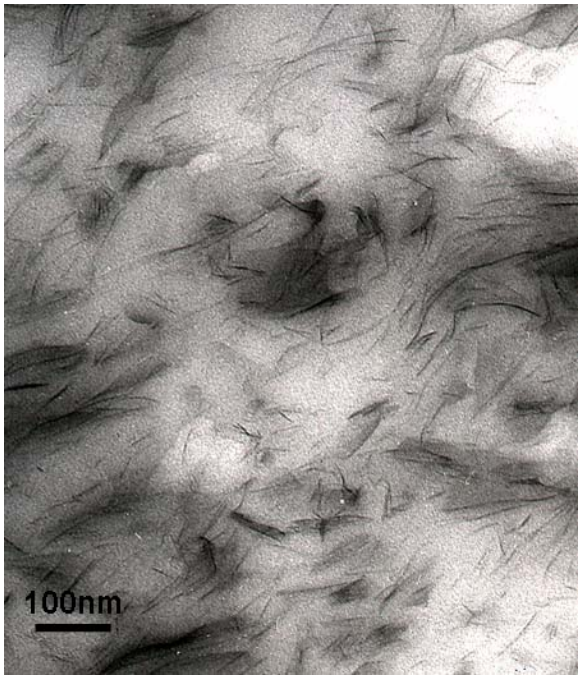

Fig. 3.4(b) TEM photomicrographs of nylon 6/clay nanocomposites prepared by melt compounding process and shaped by injection molding machine in 50,000 magnification.

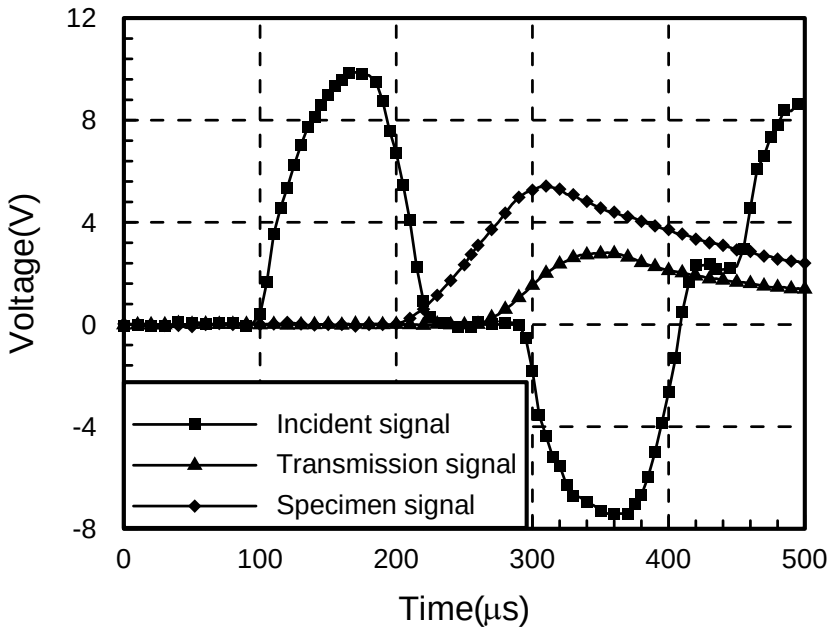

Fig. 3.5(a) Strain gage signals recorded in SHPB test for dry nylon 6.

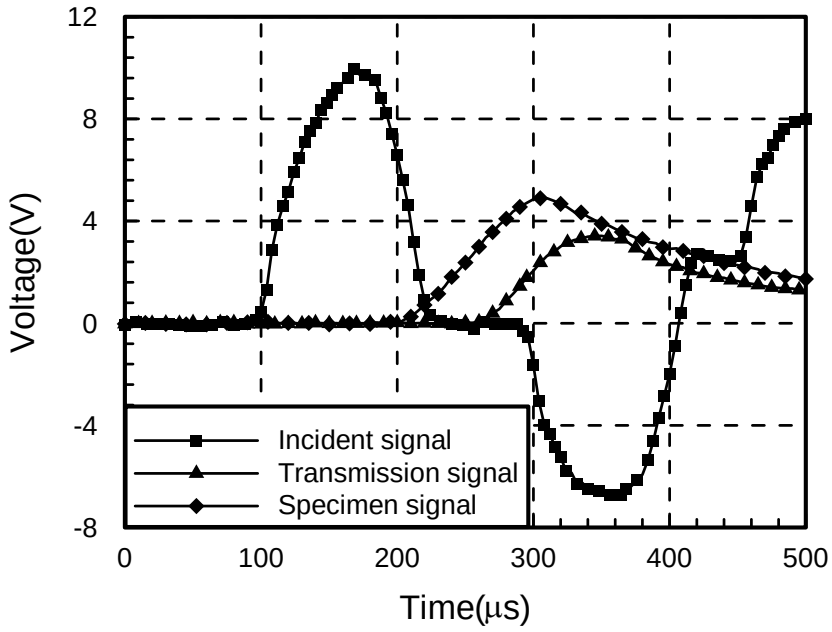

Fig. 3.5(b) Strain gage signals recorded in SHPB test for dry nylon 6/clay nanocomposites.

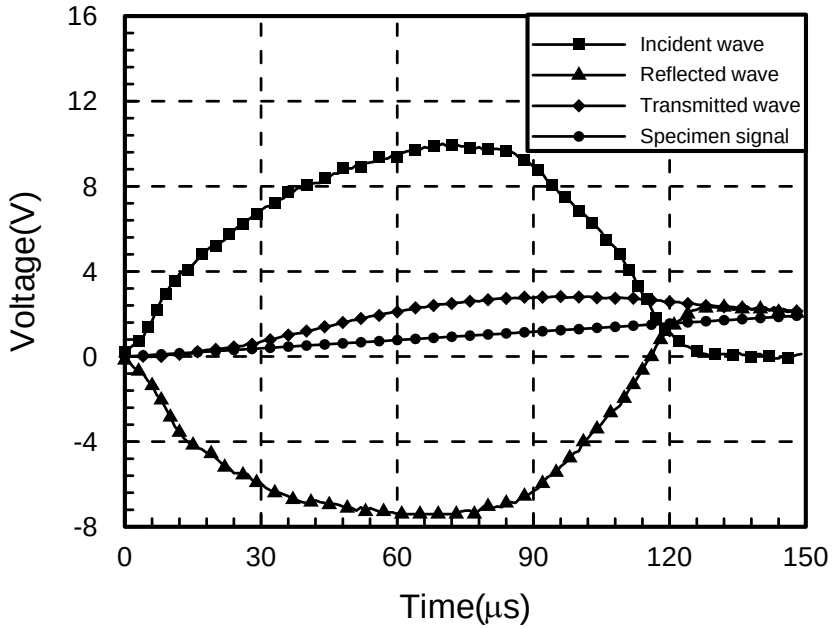

Fig. 3.6(a) Time shift for strain gage signals recorded in SHPB test for dry nylon 6.

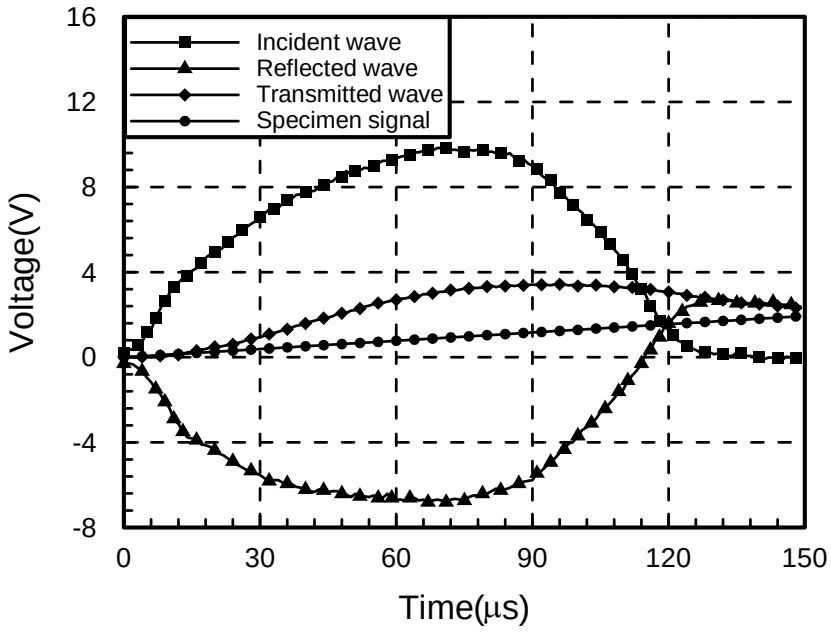

Fig. 3.6(b) Time shift for strain gage signals recorded in SHPB test for dry nylon 6/clay nanocomposites.

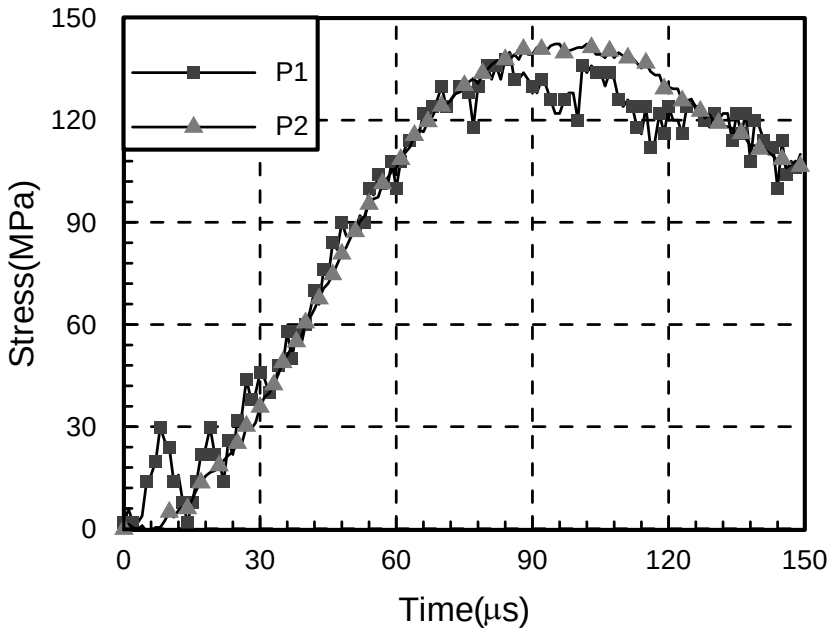

Fig. 3.7(a) Time histories of the contact stresses for dry nylon 6 in SHPB tests.

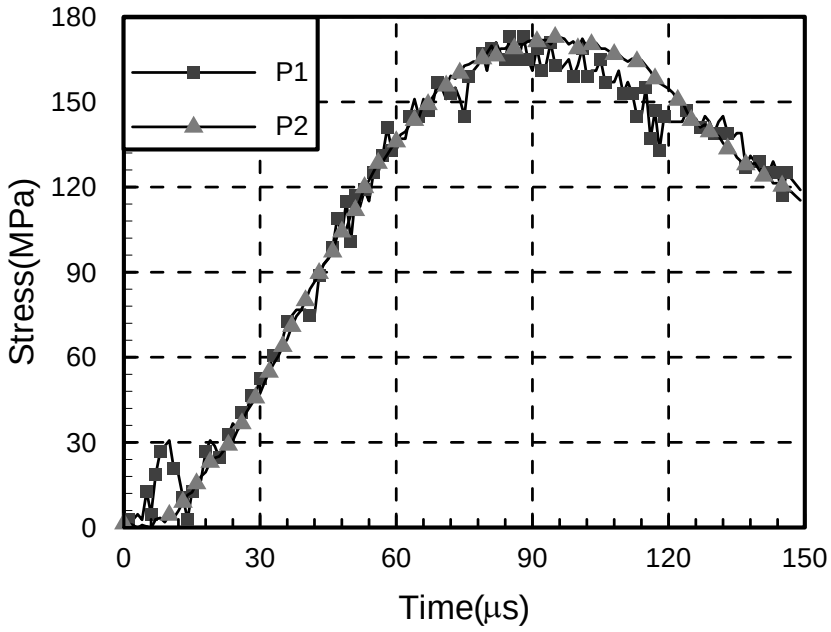

Fig. 3.7(b) Time histories of the contact stresses for dry nylon 6/clay nanocomposites in SHPB tests.

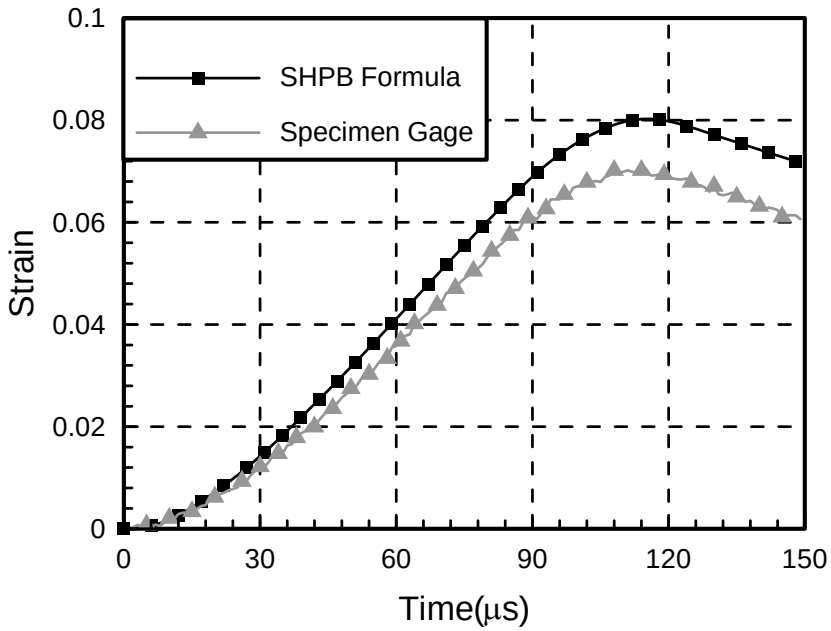

Fig. 3.8(a) Strain history obtained from Hopkinson bar formula and strain gage signals for dry nylon 6 in SHPB tests.

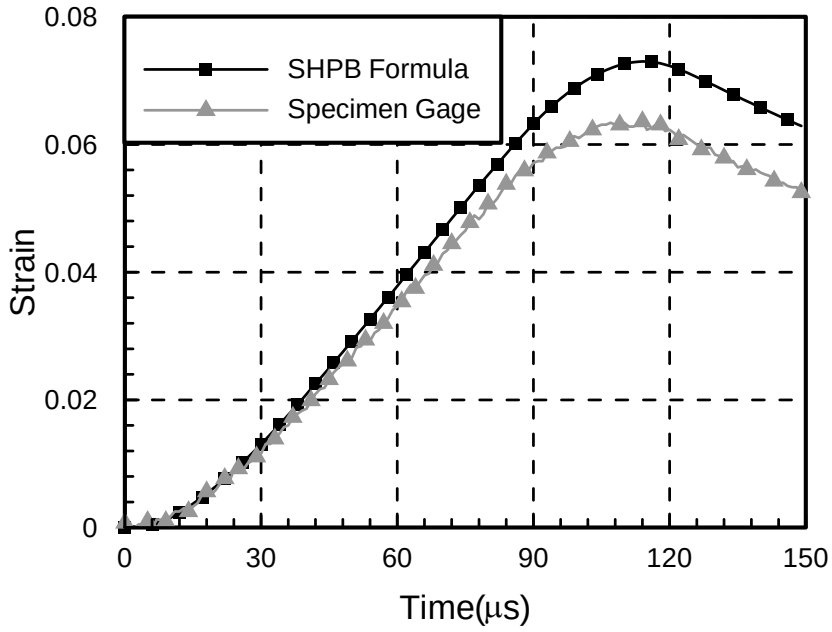

Fig. 3.8(b) Strain history obtained from Hopkinson bar formula and strain gage signals for dry nylon 6/clay nanocomposites in SHPB tests.

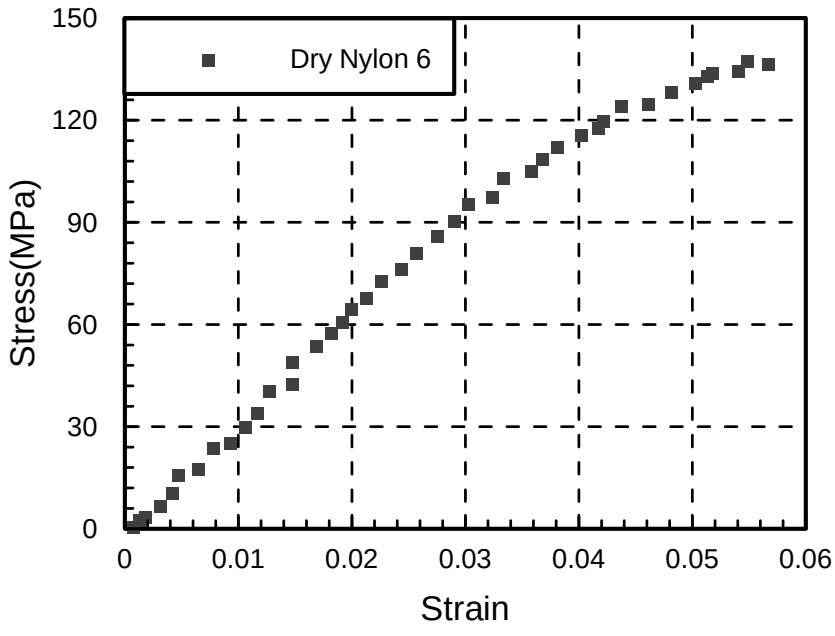

Fig. 3.9(a) The stress-strain curve of dry nylon 6 specimen (800/s).

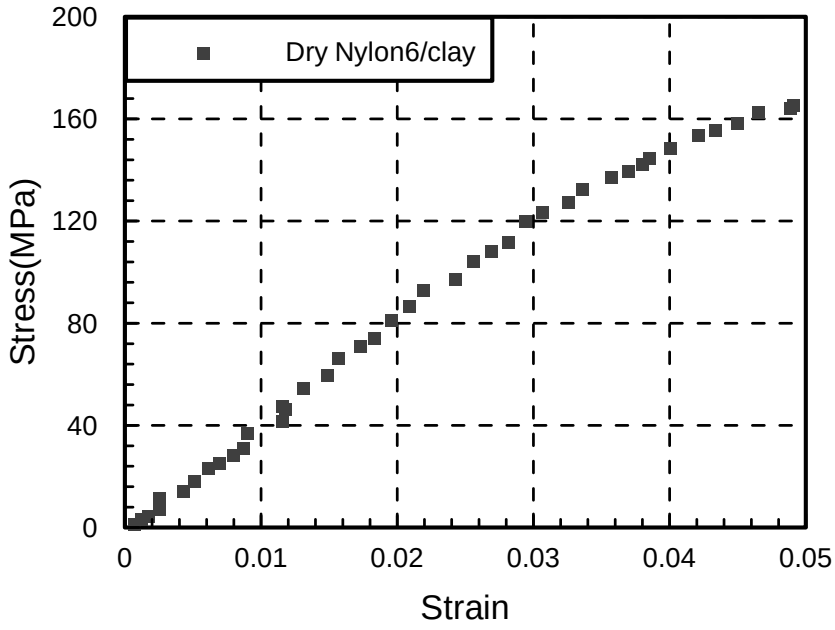

Fig. 3.9(b) The stress-strain curve of dry nylon 6/clay nanocomposites specimen (800/s).

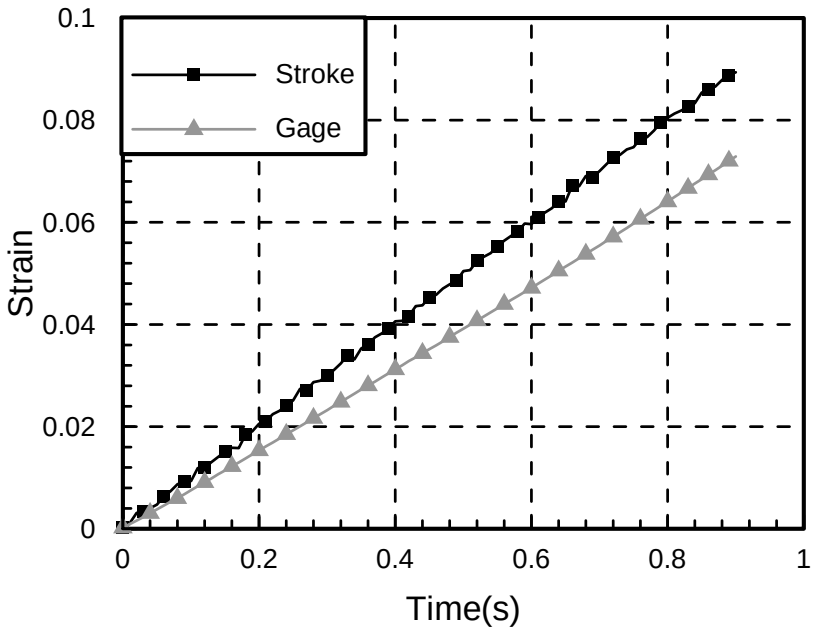

Fig. 3.10(a) Comparison of dry nylon 6 specimen strain recorded by gages result with derived from MTS stroke result under intermediate strain rate (8×10^{-2}/s).

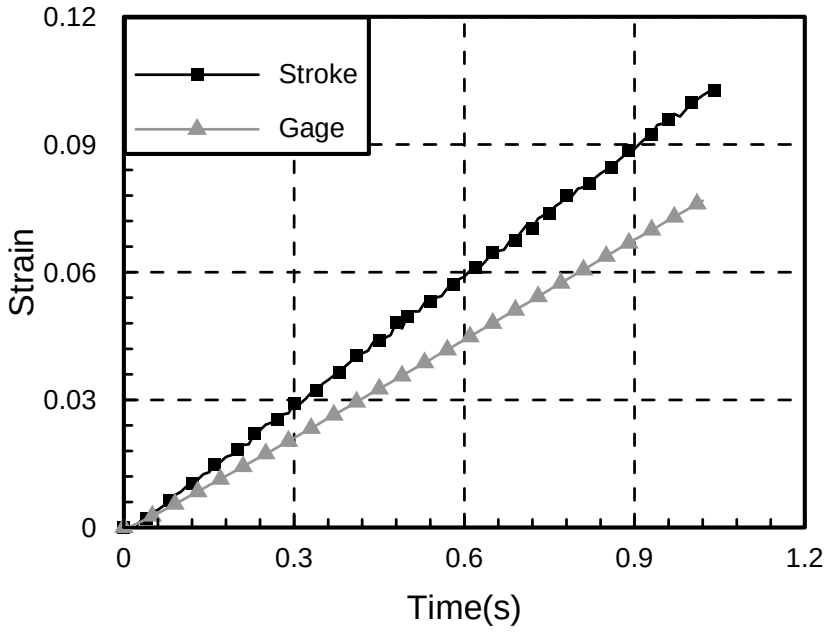

Fig. 3.10(b) Comparison of dry nylon 6/clay nanocomposites specimen strain recorded by gages result with derived from MTS stroke result under intermediate strain rate (8×10^{-2}/s).

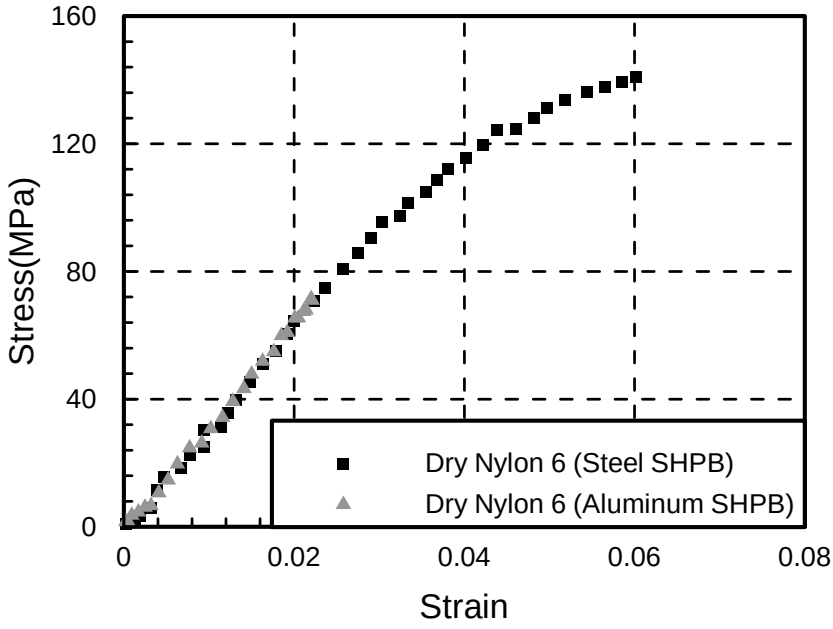

Fig. 3.11(a) Comparison of stress-strain curve of dry nylon 6 by using steel SHPB apparatus with aluminum SHPB apparatus.

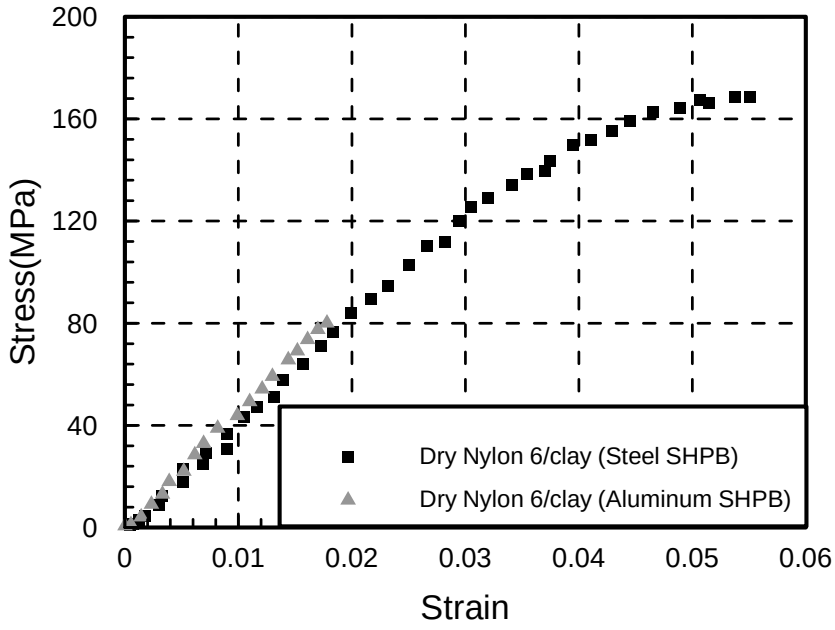

Fig. 3.11(b) Comparison of stress-strain curve of dry nylon 6/clay nanocomposites by using steel SHPB apparatus with aluminum SHPB apparatus.

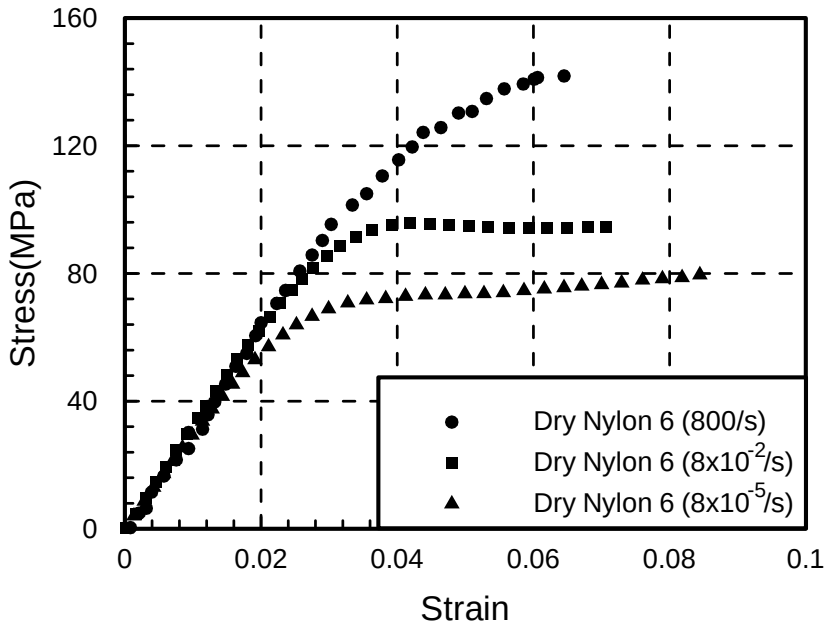

Fig. 3.12(a) Comparison of stress-strain curves of dry nylon 6 under different strain rate tests.

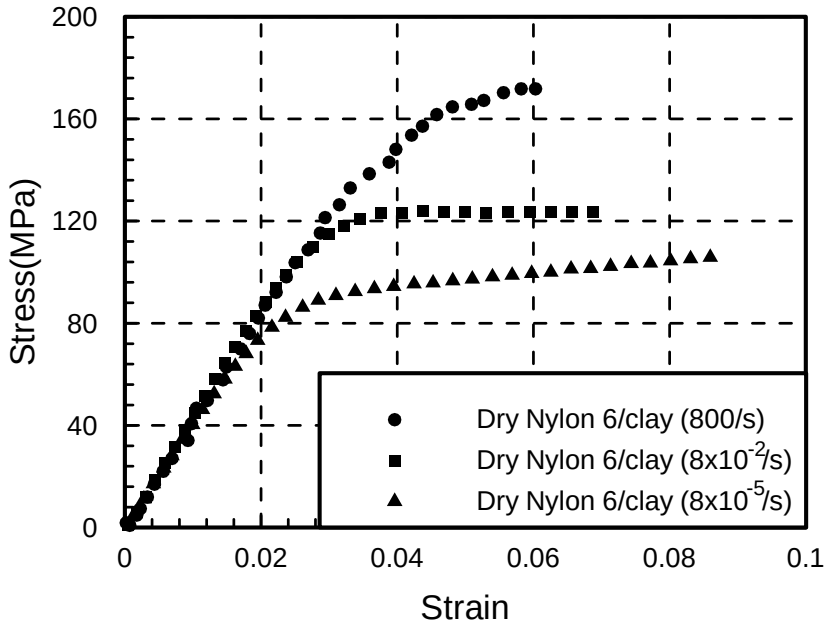

Fig. 3.12(b) Comparison of stress-strain curves of dry nylon 6/clay nanocomposites under different strain rate tests.

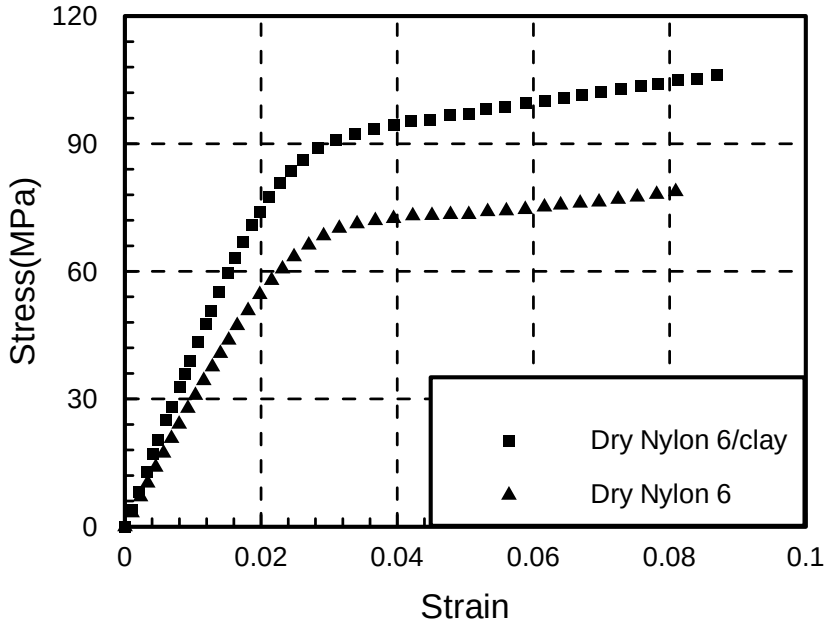

Fig. 3.13. Stress-strain curves for dry nylon 6 and dry nylon 6/clay nanocomposites under true strain rate of 8×10^{-5}/s.

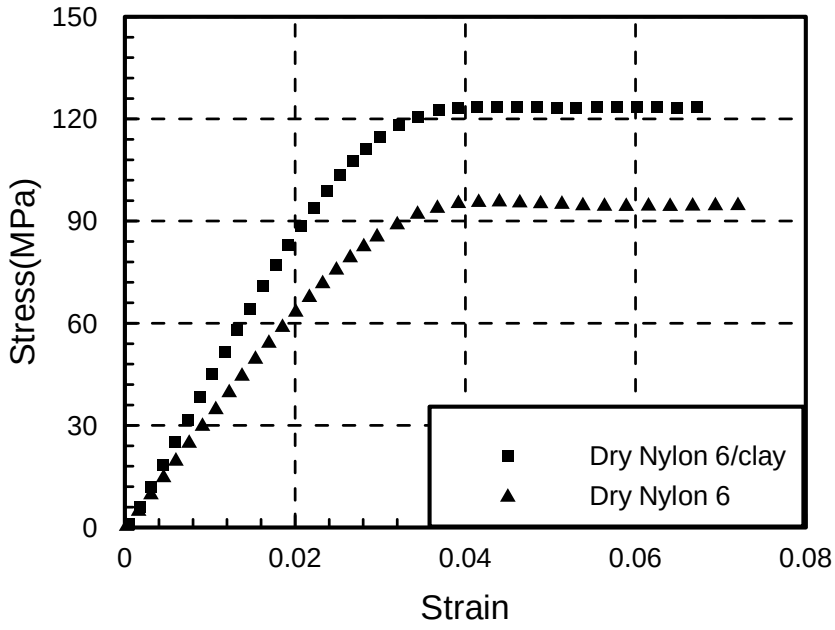

Fig. 3.14. Stress-strain curves for dry nylon 6 and dry nylon 6/clay nanocomposites under true strain rate of 8×10^{-2}/s.

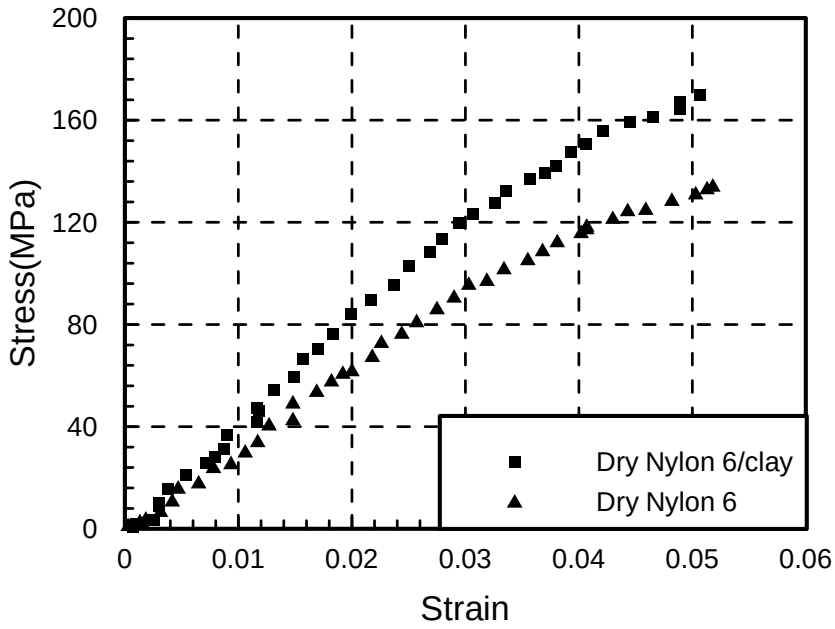

Fig. 3.15. Stress-strain curves for dry nylon 6 and dry nylon 6/clay nanocomposites under strain rate of 800/s (steel SHPB).

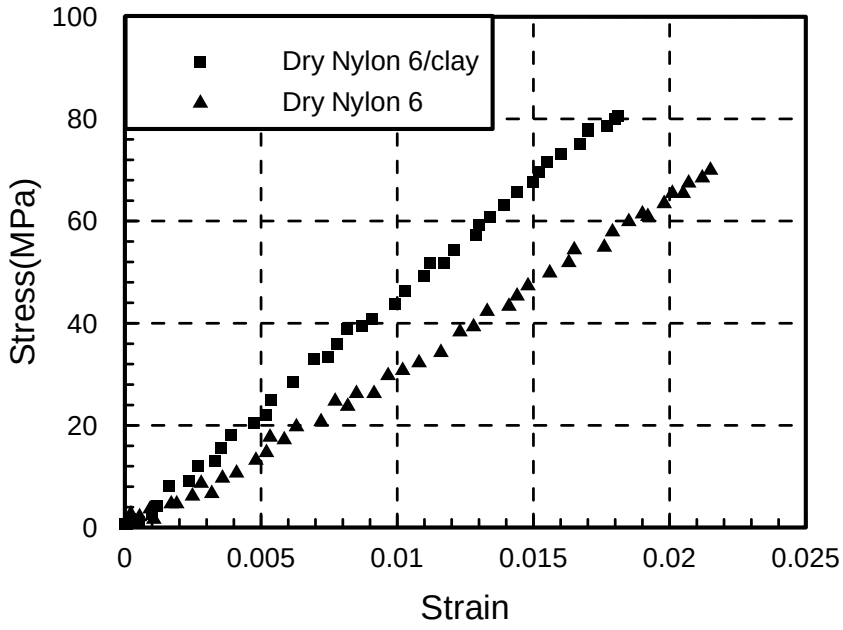

Fig. 3.16. Stress-strain curves for dry nylon 6 and dry nylon 6/clay nanocomposites under strain rate of 500/s (aluminum SHPB).

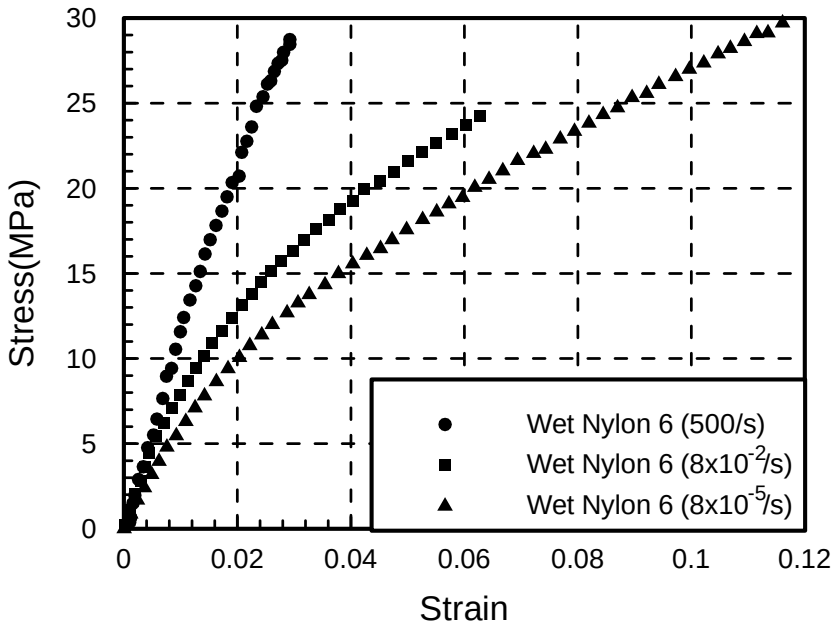

Fig. 3.17(a) Comparison of stress-strain curves of wet nylon 6 under different strain rate tests.

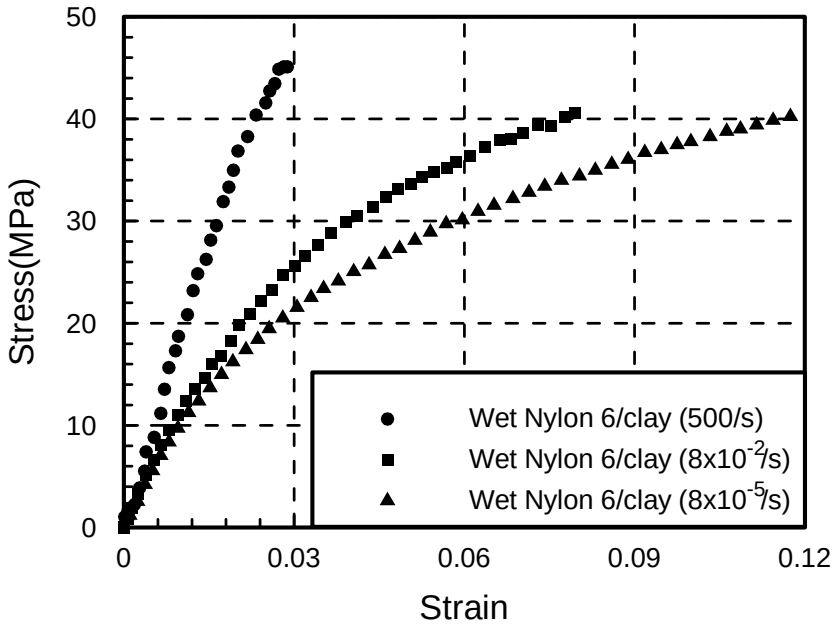

Fig. 3.17(b) Comparison of stress-strain curves of wet nylon 6/clay nanocomposites under different strain rate tests.

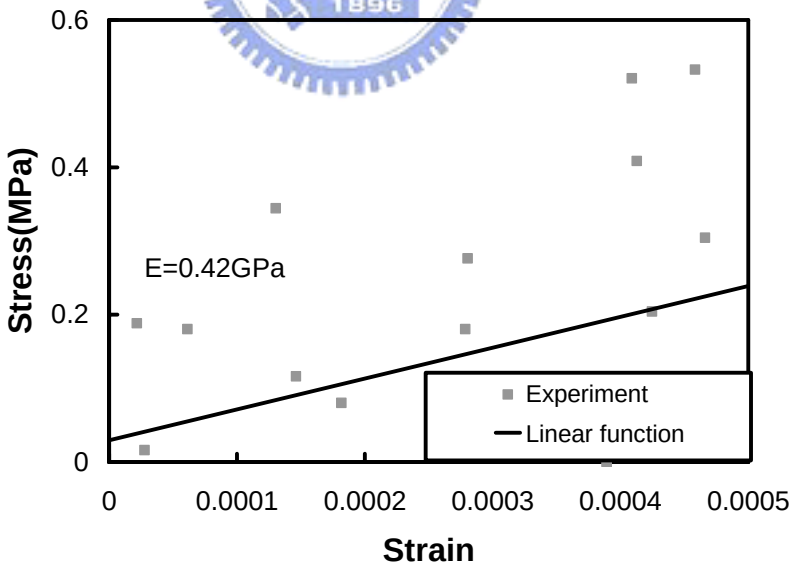

Fig. 3.18. Determination of Young's modulus of wet nylon6 (test1) under strain range of 0.05% at true strain rate of 8×10^{-5}/s.

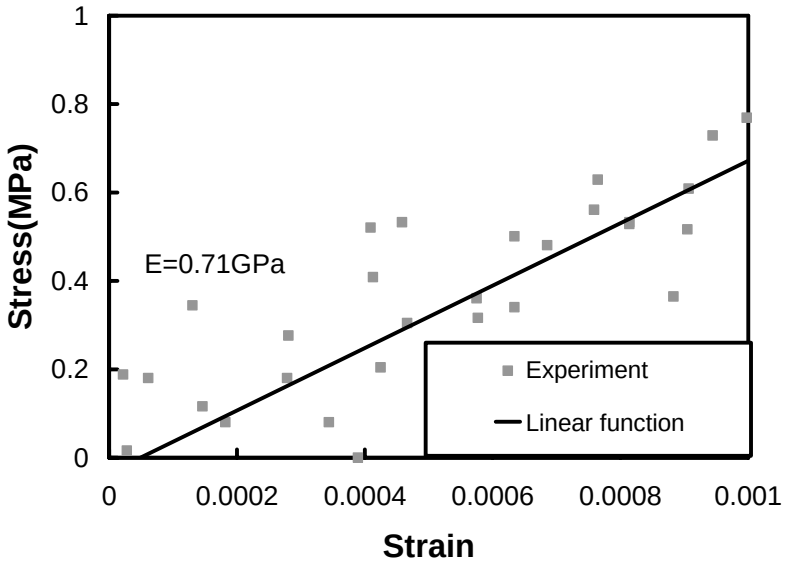

Fig. 3.19. Determination of Young's modulus of wet nylon6 (test1) under strain range of 0.1% at true strain rate of 8×10^{-5}/s.

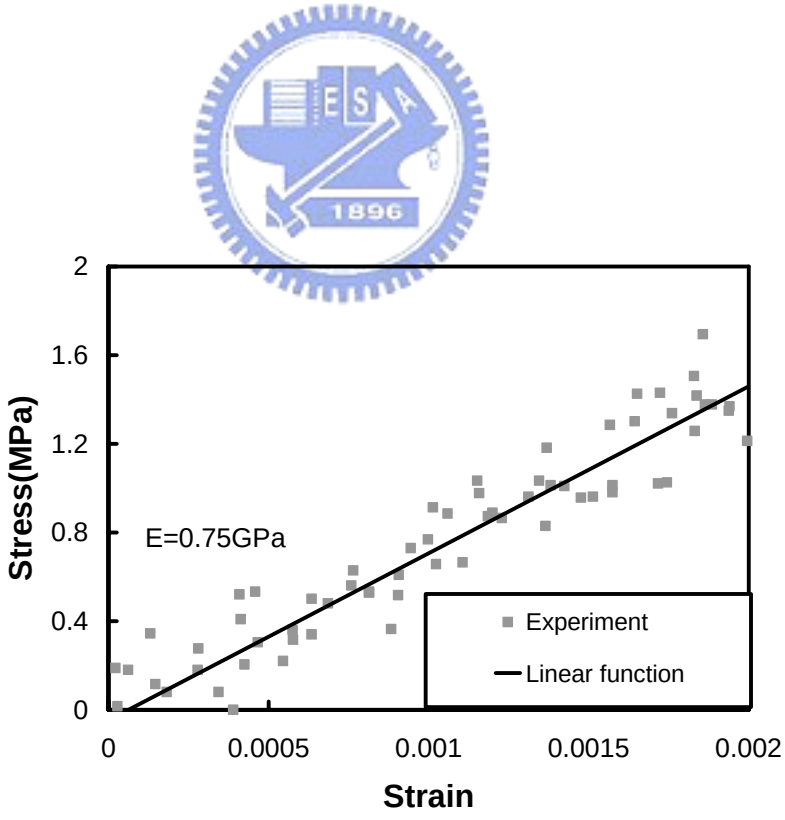

Fig. 3.20. Determination of Young's modulus of wet nylon6 (test1) under strain range of 0.2% at true strain rate of 8×10^{-5}/s.

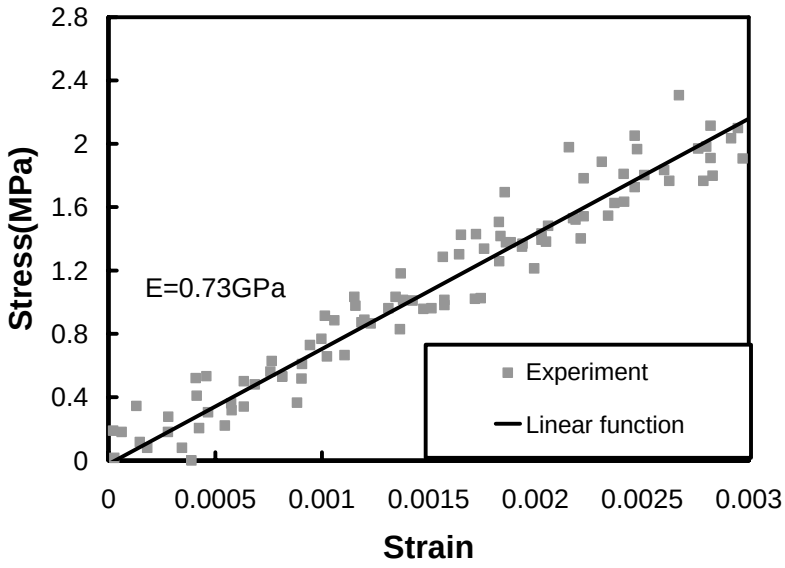

Fig. 3.21. Determination of Young's modulus of wet nylon6 (test1) under strain range of 0.3% at true strain rate of 8×10^{-5}/s.

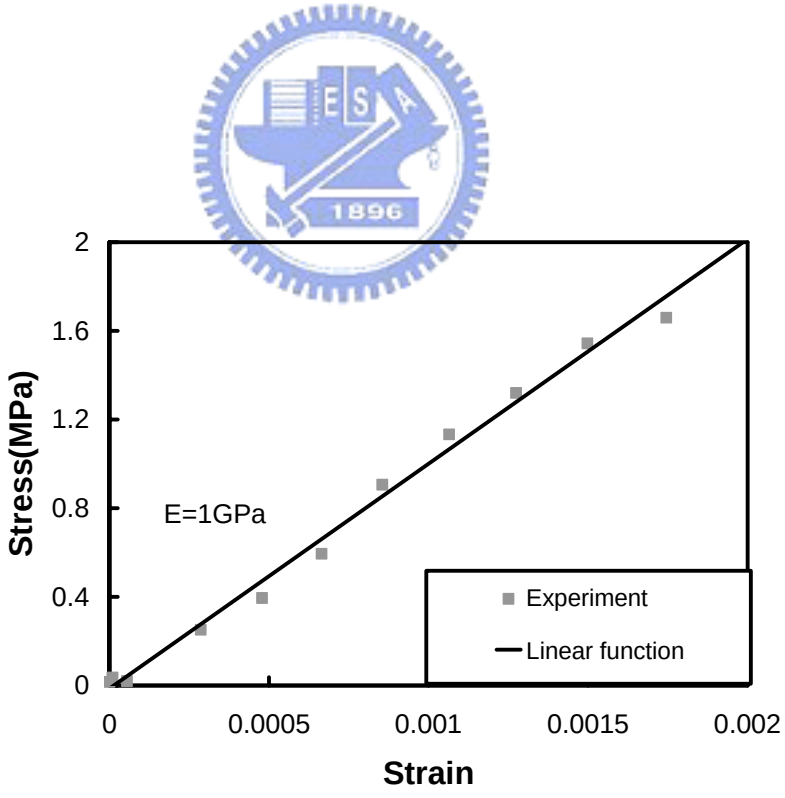

Fig. 3.22(a) Determination of Young's modulus of wet nylon6 at true strain rate of 0.08/s.

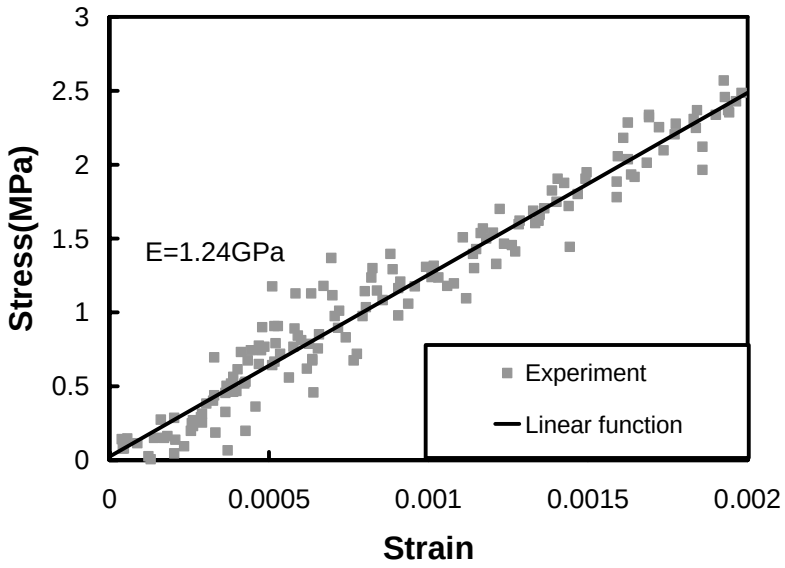

Fig. 3.22(b) Determination of Young's modulus of wet nylon6/clay nanocomposites at true strain rate of 0.08/s.

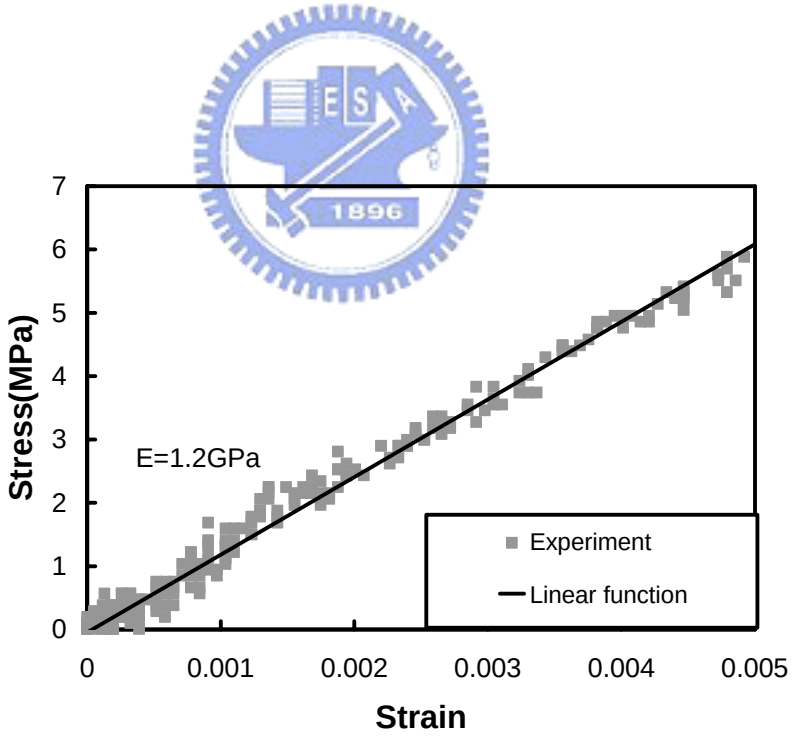

Fig. 3.23(a) Determination of Young's modulus of wet nylon6 at strain rate of 500/s.

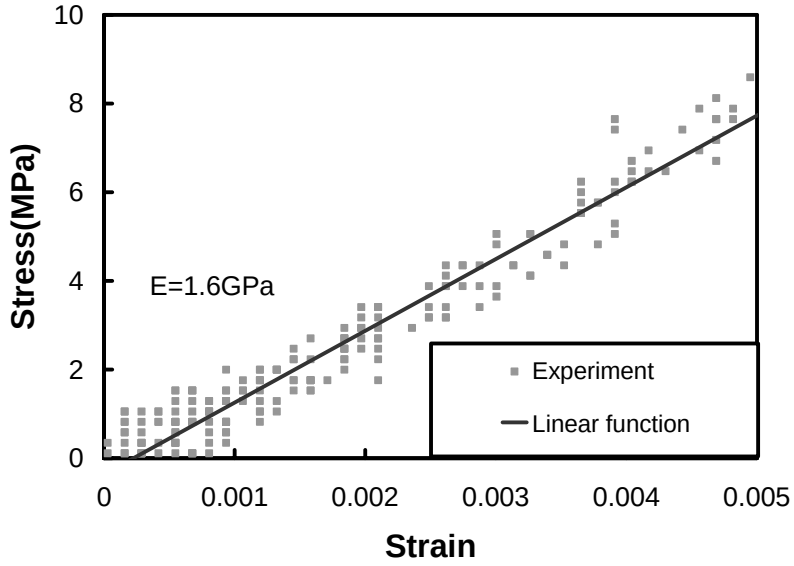

Fig. 3.23(b) Determination of Young's modulus of wet nylon6/clay nanocomposites at strain rate of 500/s.

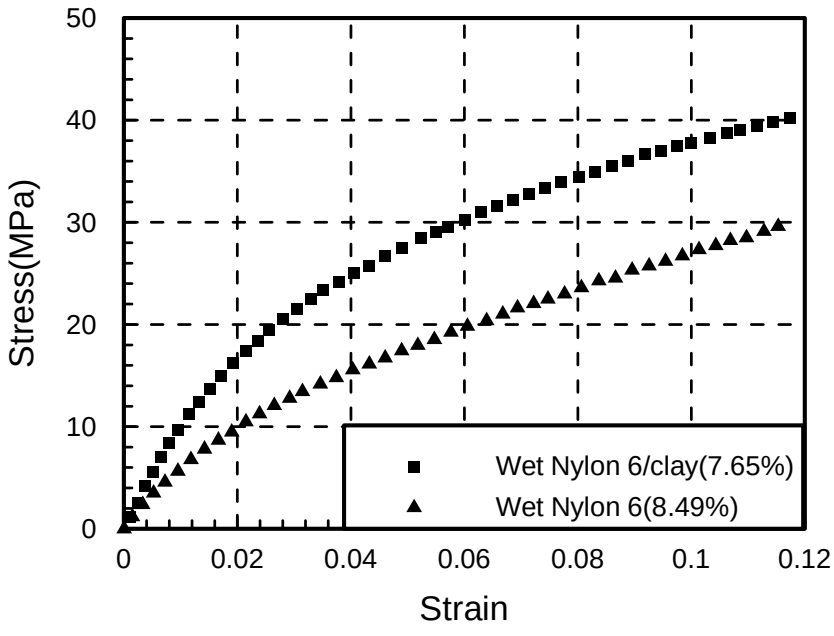

Fig. 3.24. Stress-strain curves for wet nylon 6 and wet nylon 6/clay nanocomposites under true strain rate of 8×10^{-5}/s.

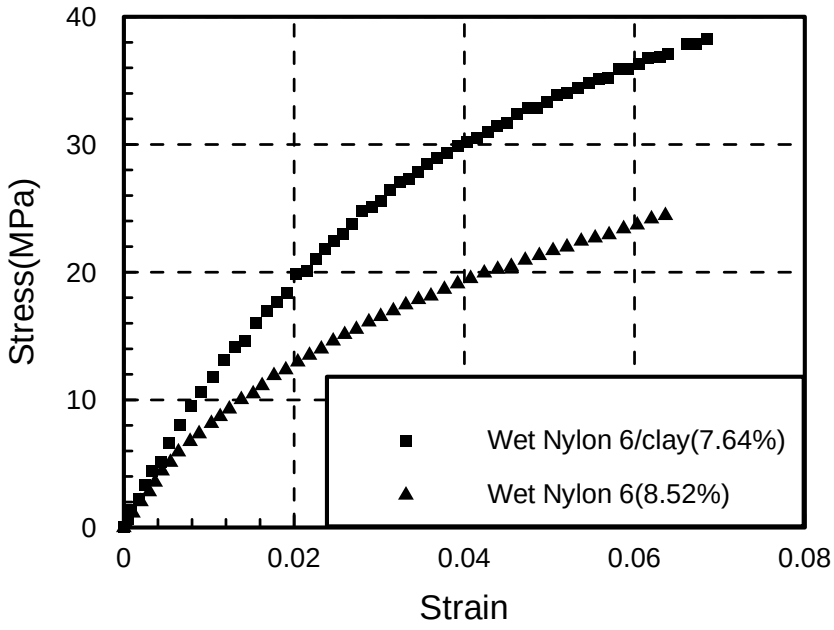

Fig. 3.25. Stress-strain curves for wet nylon 6 and wet nylon 6/clay nanocomposites under true strain rate of 8×10^{-2}/s.

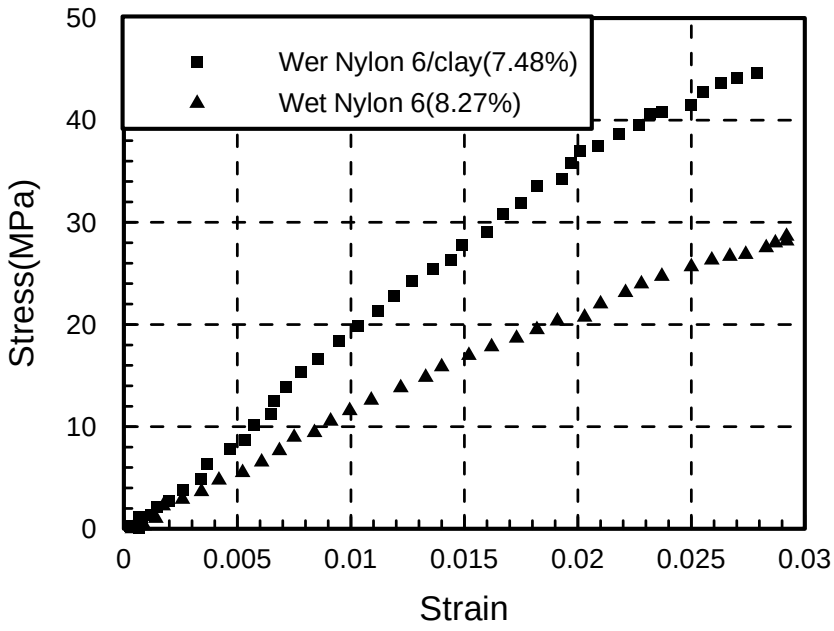

Fig. 3.26. Stress-strain curves for wet nylon 6 and wet nylon 6/clay nanocomposites under strain rate of 500/s.

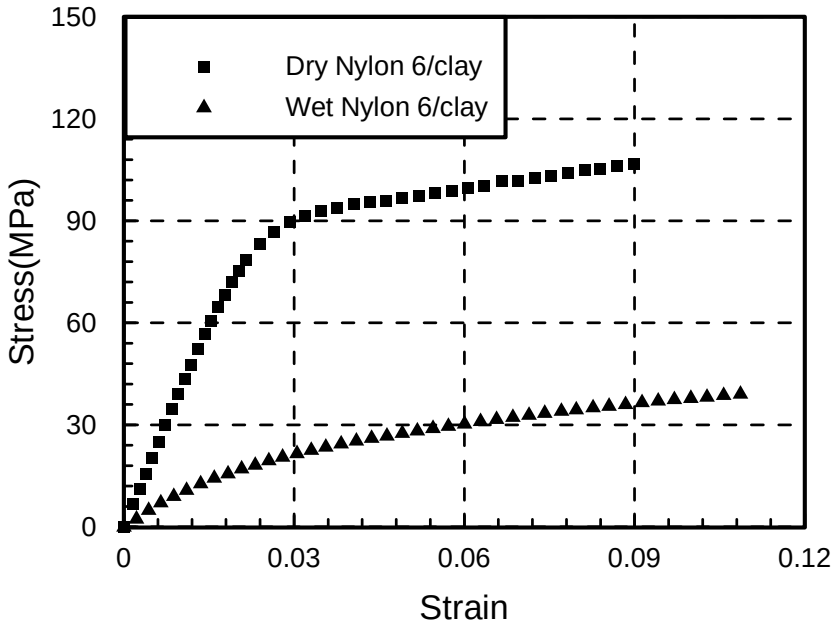

Fig. 3.27. Comparison of stress-strain curves of dry nylon 6/clay nanocomposite specimen with wet specimen at true strain rate of 8×10^{-5}/s.

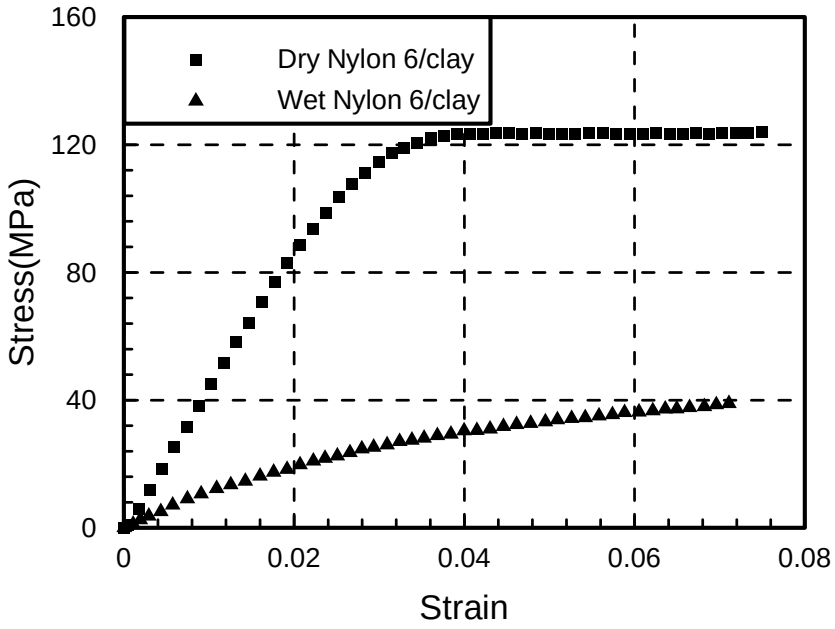

Fig. 3.28. Comparison of stress-strain curves of dry nylon 6/clay nanocomposite specimen with wet specimen at true strain rate of 8×10^{-2}/s.

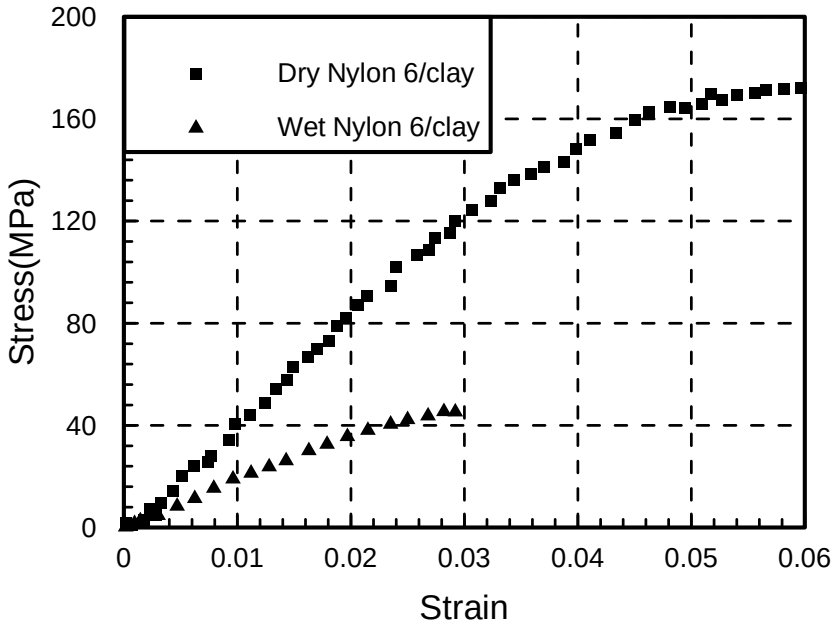

Fig. 3.29. Comparison of stress-strain curves of dry nylon 6/clay nanocomposite specimen with wet specimen at strain rate of 500/s.

Appendix A

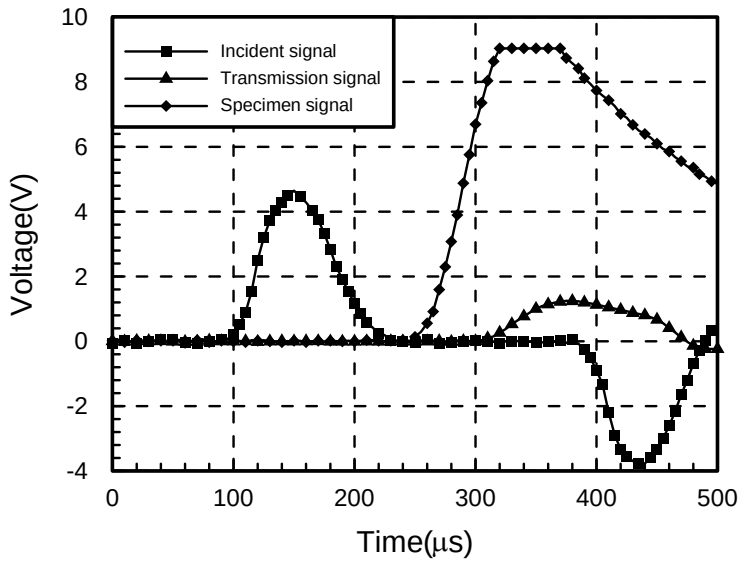

Fig. A1. Strain gage signals recorded in SHPB test for wet nylon6.

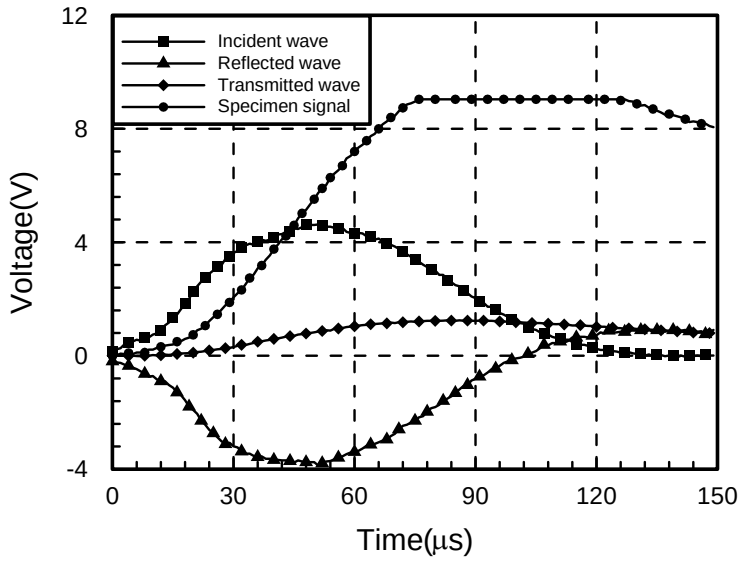

Fig. A2. Time shift for strain gage signals recorded in SHPB test for wet nylon6.

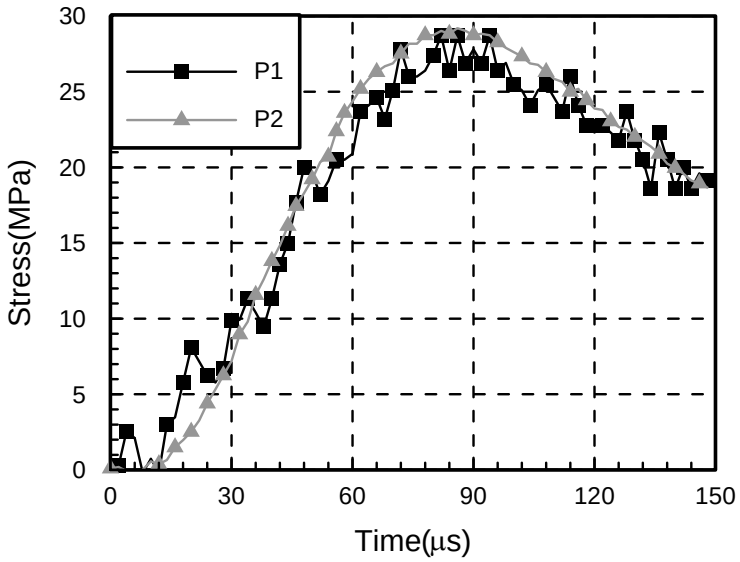

Fig. A3. Time histories of the contact stresses for wet nylon6 in SHPB tests.

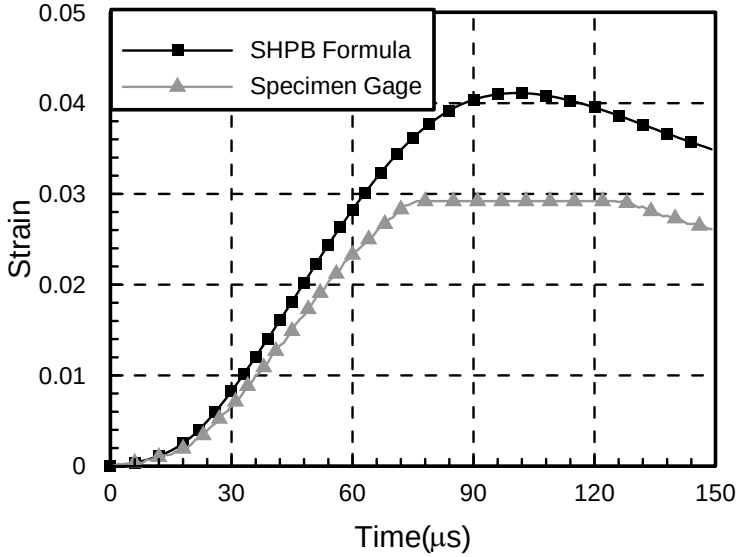

Fig. A4. Strain history obtained from Hopkinson bar formula and strain gage signals for wet nylon6 in SHPB tests.

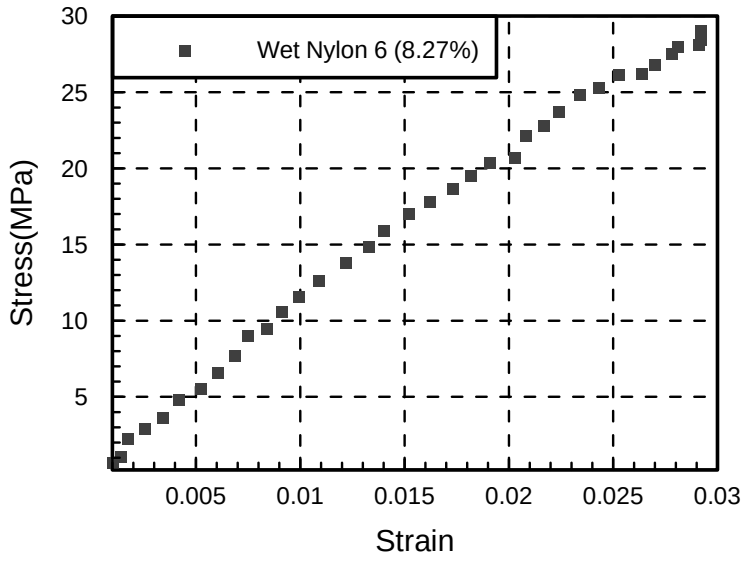

Fig. A5. The stress-strain curve of wet nylon 6 specimen (500/s).

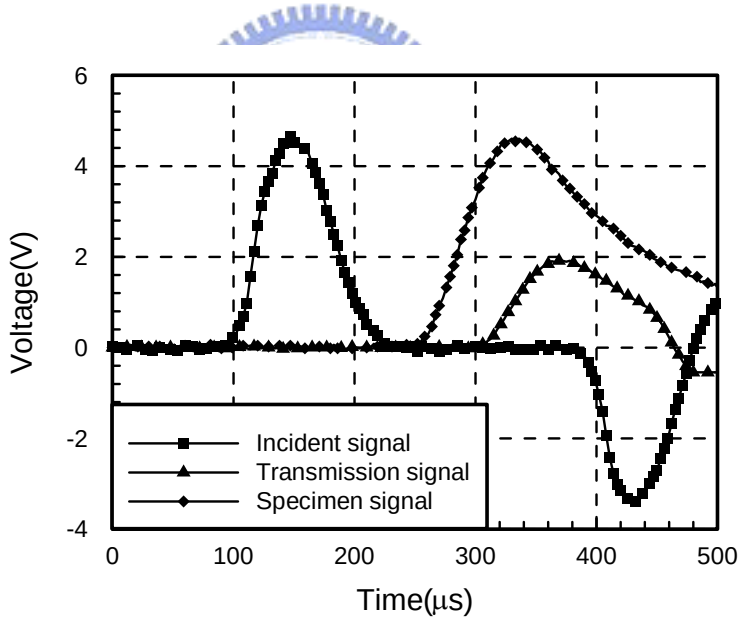

Fig. A6. Strain gage signals recorded in SHPB test for wet nylon6/clay nanocomposites.

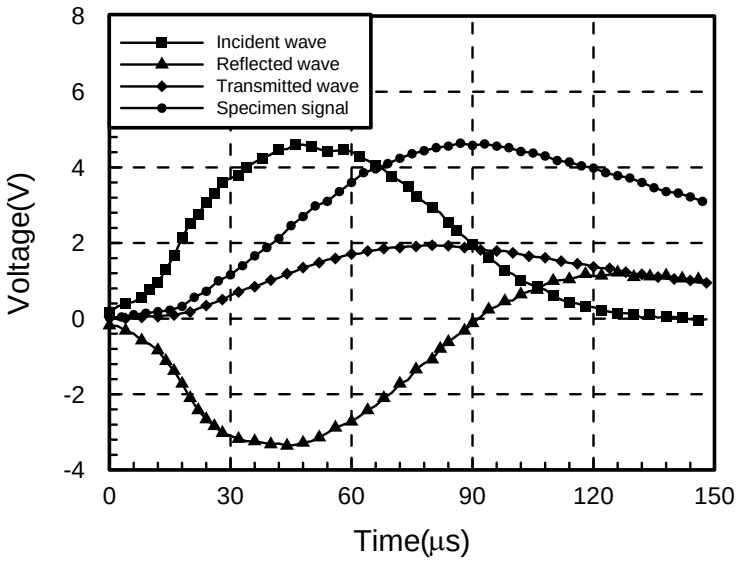

Fig. A7. Time shift for Strain gage signals recorded in SHPB test for wet nylon6/clay nanocomposites.

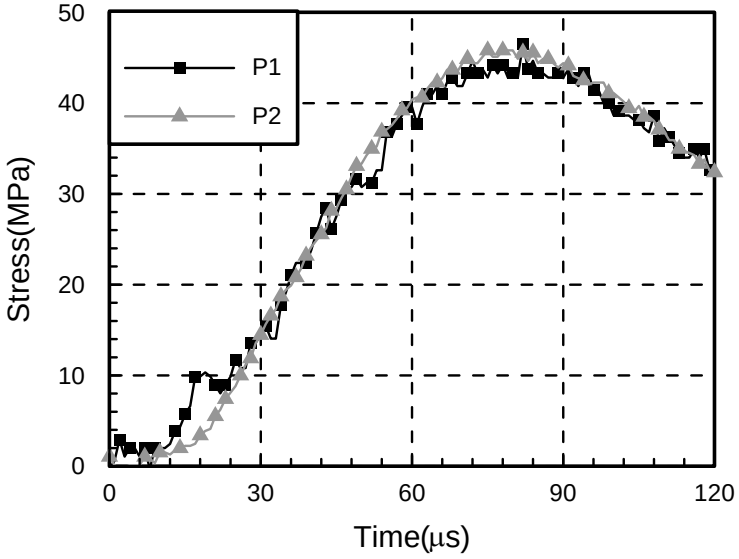

Fig. A8. Time histories of the contact stresses for wet nylon6/clay nanocomposites in SHPB tests.

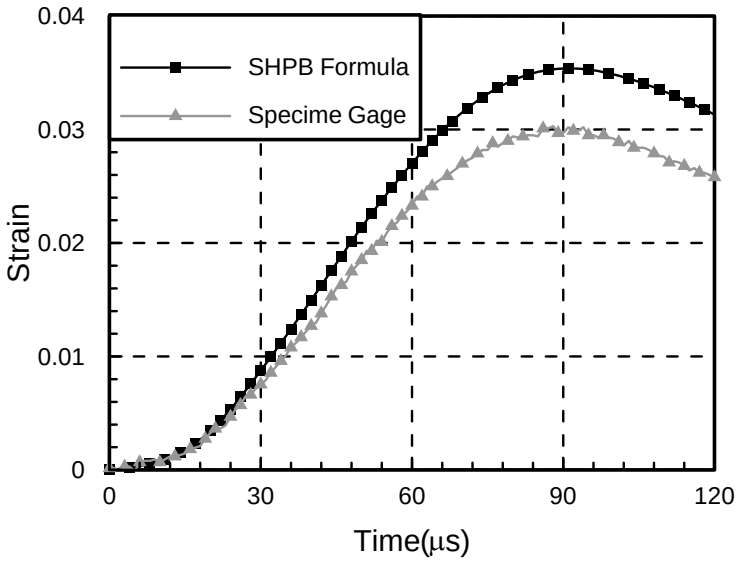

Fig. A9. Strain history obtained from Hopkinson bar formula and strain gage signals for wet nylon6/clay nanocomposites in SHPB tests

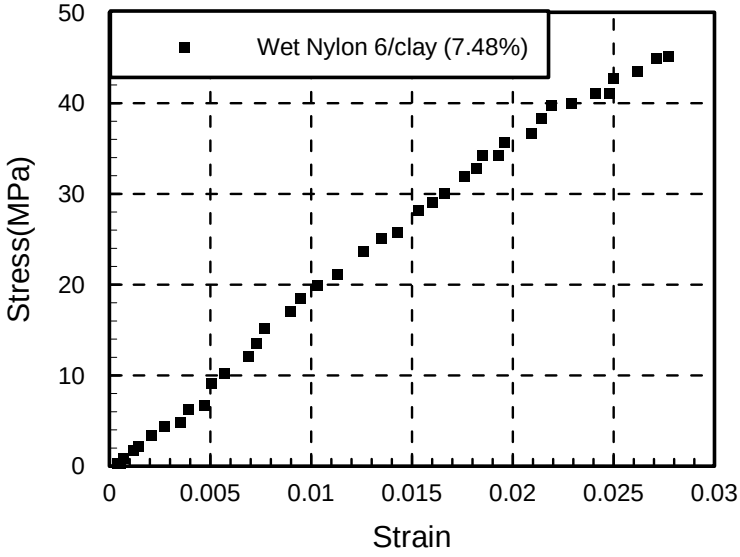

Fig. A10. The stress-strain curve of wet nylon 6/clay nanocomposites specimen (500/s).

Appendix B

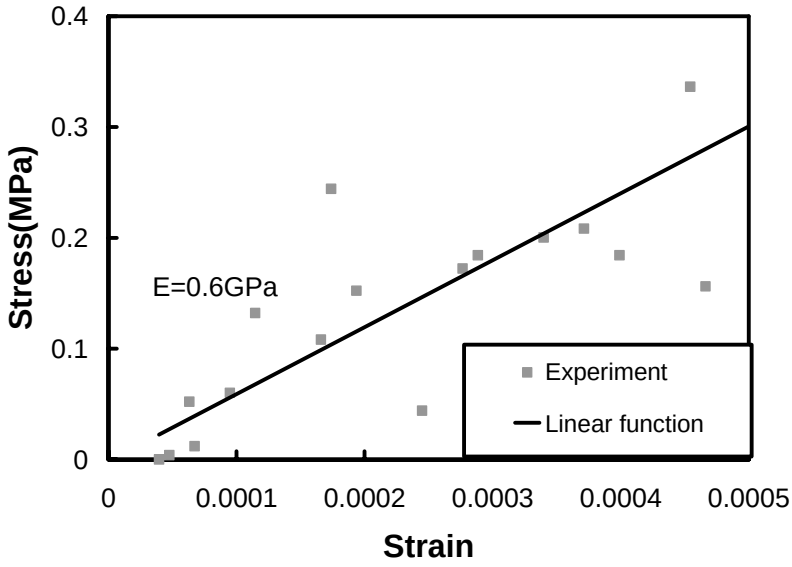

Fig. B1. Determination of Young's modulus of wet nylon6 (test2) under strain range of 0.05% at true strain rate of 8×10^{-5}/s.

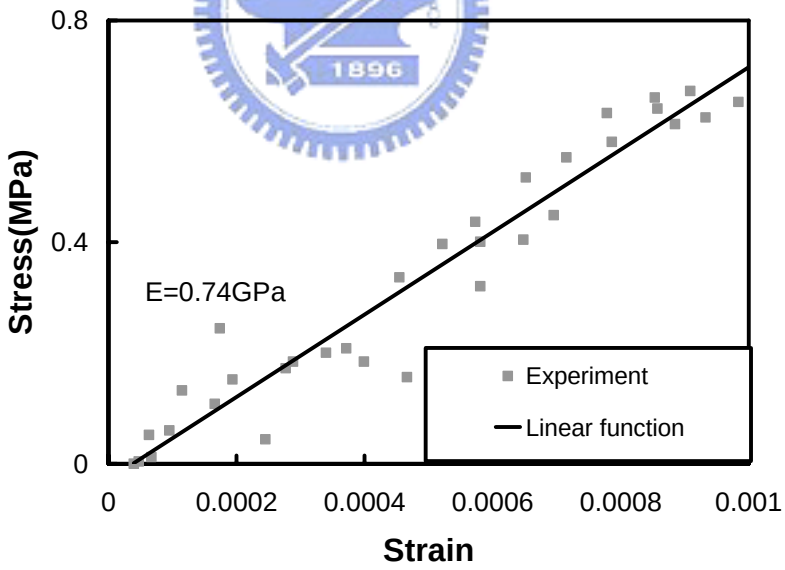

Fig. B2. Determination of Young's modulus of wet nylon6 (test2) under strain range of 0.1% at true strain rate of 8×10^{-5}/s.

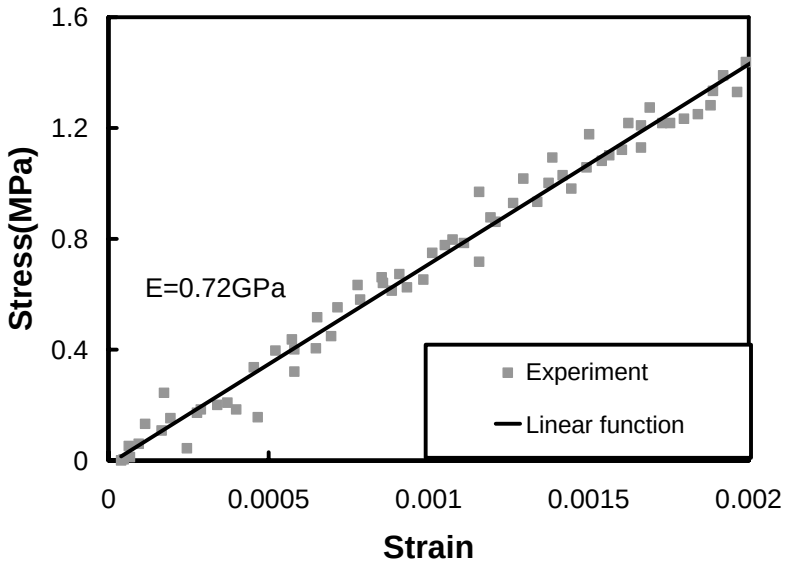

Fig. B3. Determination of Young's modulus of wet nylon6 (test2) under strain range of 0.2% at true strain rate of 8×10^{-5}/s.

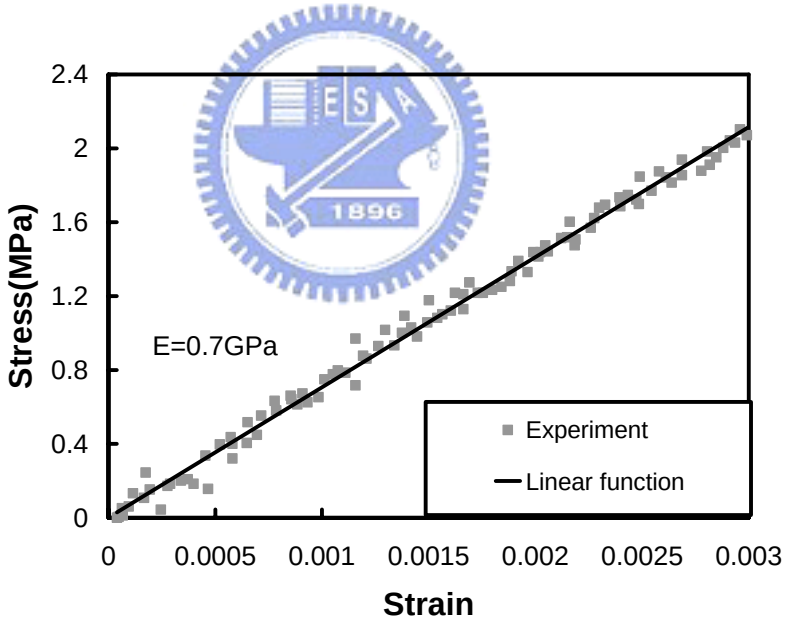

Fig. B4. Determination of Young's modulus of wet nylon6 (test2) under strain range of 0.3% at true strain rate of 8×10^{-5}/s.

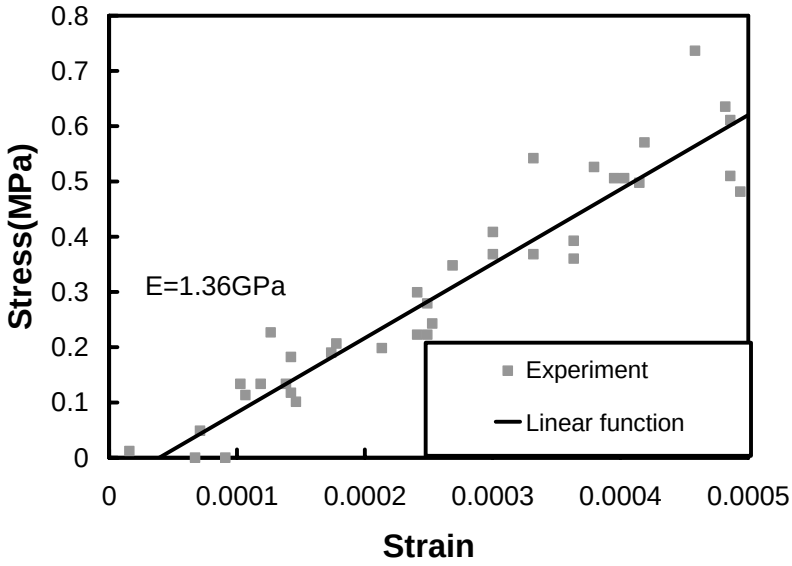

Fig. B5. Determination of Young's modulus of wet nylon6/clay (test1) under strain range of 0.05% at true strain rate of 8×10^{-5}/s.

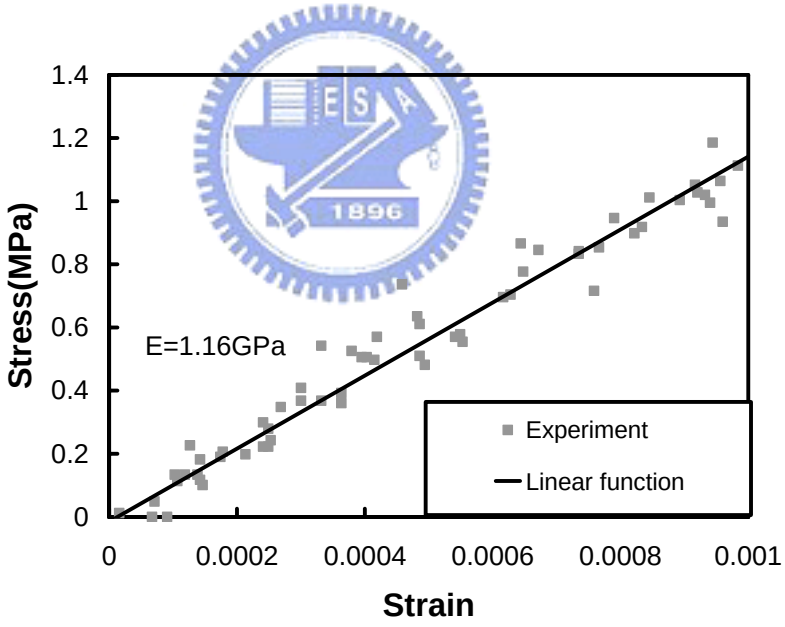

Fig. B6. Determination of Young's modulus of wet nylon6/clay (test1) under strain range of 0.1% at true strain rate of 8×10^{-5}/s.

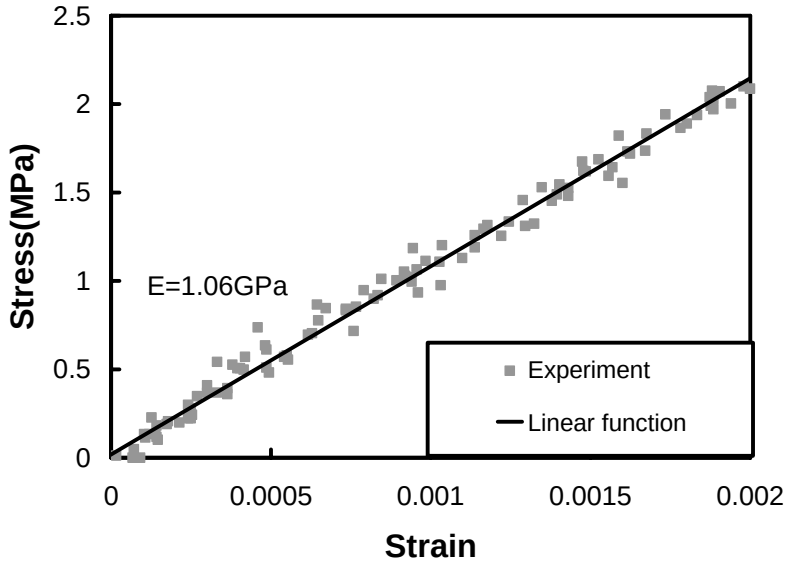

Fig. B7. Determination of Young's modulus of wet nylon6/clay (test1) under strain range of 0.2% at true strain rate of 8×10^{-5}/s.

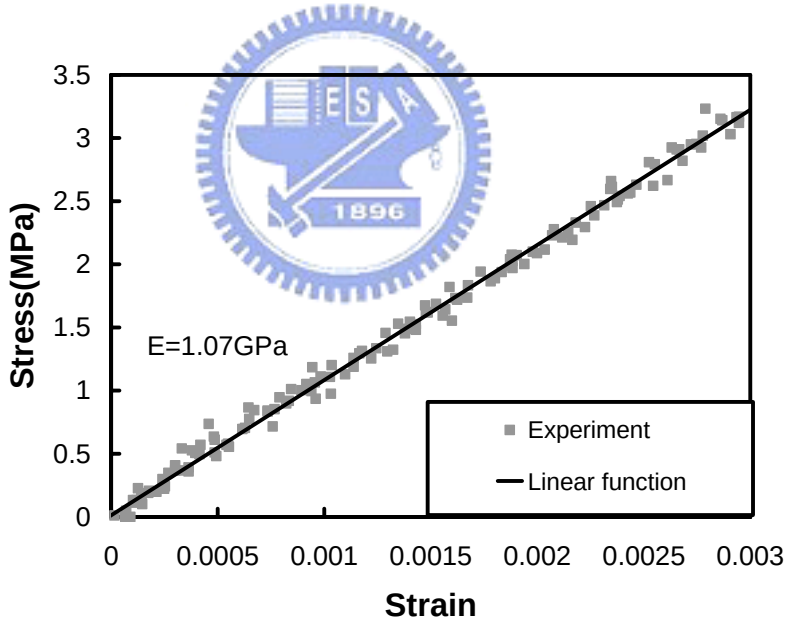

Fig. B8. Determination of Young's modulus of wet nylon6/clay (test1) under strain range of 0.3% at true strain rate of 8×10^{-5}/s.

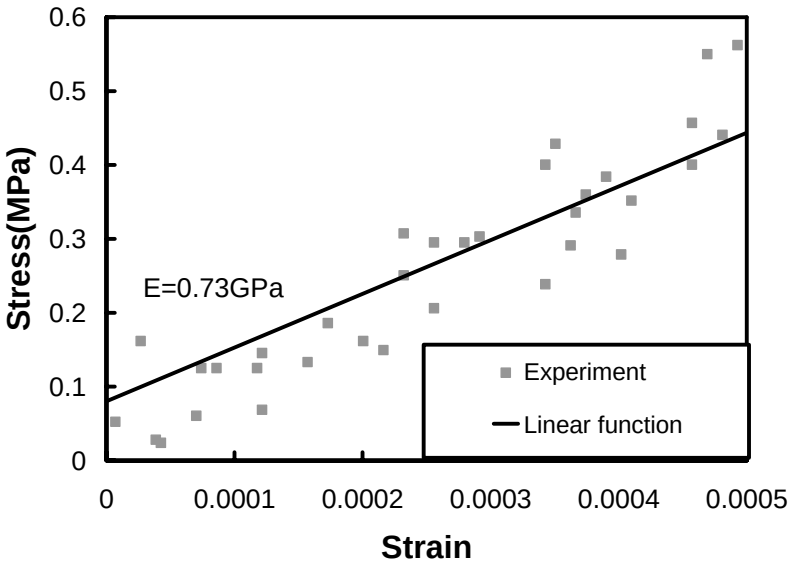

Fig. B9. Determination of Young's modulus of wet nylon6/clay (test2) under strain range of 0.05% at true strain rate of 8×10^{-5}/s.

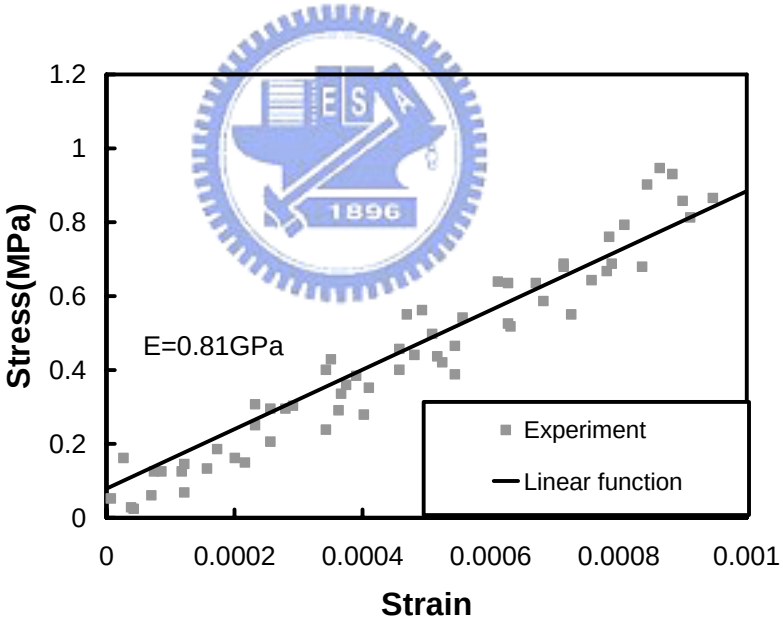

Fig. B10. Determination of Young's modulus of wet nylon6/clay (test2) under strain range of 0.1% at true strain rate of 8×10^{-5}/s.

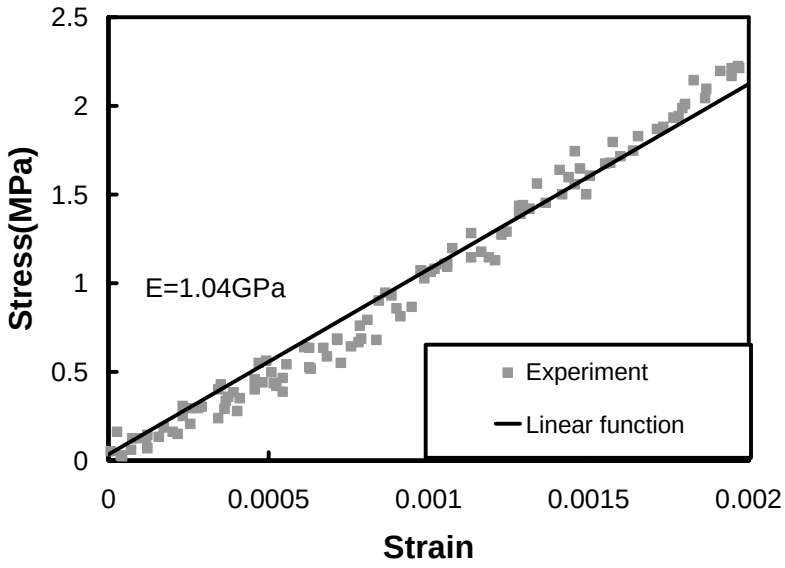

Fig. B11. Determination of Young's modulus of wet nylon6/clay (test2) under strain range of 0.2% at true strain rate of 8×10^{-5}/s.

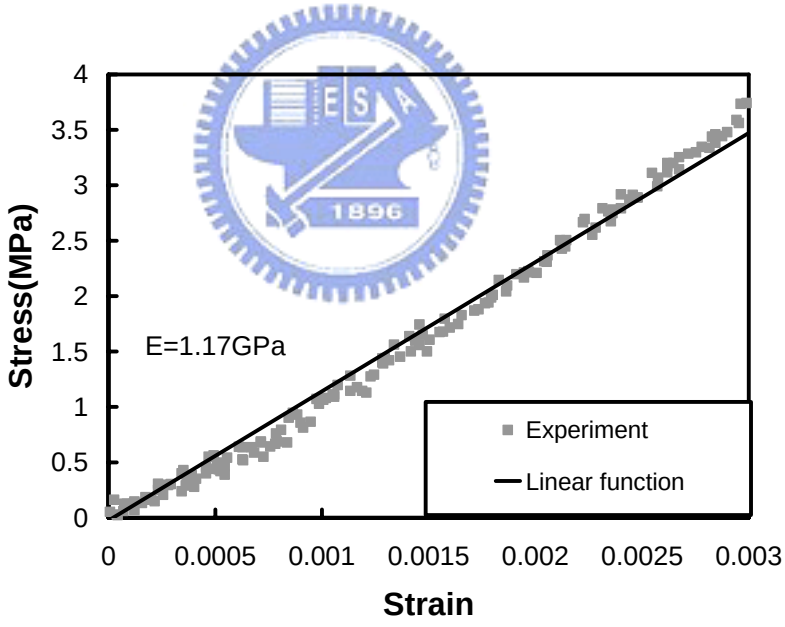

Fig. B12. Determination of Young's modulus of wet nylon6/clay (test2) under strain range of 0.3% at true strain rate of 8×10^{-5}/s.